Human IFN-g immunity to mycobacteria is governed by both IL-12 and IL-23

Markle, Janet G. … [et al.]

Science Immunology, 21 Dec 2018

Vol. 3, Issue 30, eaau6759

Published version: https://dx.doi.org/10.1126/sciimmunol.aau6759

Human IFN-γ immunity to mycobacteria is governed by both IL-12 and IL-23

Janet G. Markle[1,#,a], Rubén Martínez-Barricarte[1,#,@], Cindy S. Ma[2,b], Elissa K. Deenick[2,b], Noé Ramírez-Alejo[1,b], Federico Mele[3,b], Daniela Latorre[3,b], Seyed Alireza Mahdaviani[4,b], Caner Aytekin[5,b], Davood Mansouri[4,b], Vanessa Bryant[6,7,8,b], Fabienne Jabot-Hanin[9], Caroline Deswarte[9,10], Alejandro Nieto-Patlán[9], Laura Surace[11], Gaspard Kerner[9,10], Yuval Itan[1,12], Sandra Jovic[3], Danielle T. Avery[2], Natalie Wong[2], Geetha Rao[2], Etienne Patin[13,14,15], Satoshi Okada[16], Benedetta Bigio[1], Bertrand Boisson[1,9,10], Franck Rapaport[1], Yoann Seeleuthner[9,10], Monika Schmidt[17], Aydan Ikinciogullari[18], Figen Dogu[18], Gonul Tanir[19], Payam Tabarsi[4], Mohammed Reza Bloursaz[4], Julia K. Joseph[1], Avneet Heer[1], Xiao-Fei Kong[1], Mélanie Migaud[9,10], Tomi Lazarov[20], Frédéric Geissmann[20,21,22], Bernhard Fleckenstein[17], Cecilia Lindestam Arlehamn[23], Alessandro Sette[23,24], Anne Puel[1,9,10], Jean-François Emile[25], Esther van de Vosse[26], Lluis Quintana-Murci[13,14,15], James P. Di Santo[11], Laurent Abel[1,9,10], Stéphanie Boisson-Dupuis[1,9,10,*], Jacinta Bustamante[1,9,10,27,*], Stuart G. Tangye[2,*], Federica Sallusto[3,28,*] and Jean-Laurent Casanova[1,9,10,29,30,@]

1. St. Giles Laboratory of Human Genetics of Infectious Diseases, Rockefeller Branch, The Rockefeller University, New York, NY, USA.
2. Immunology Division, Garvan Institute of Medical Research, Sydney, Australia; St Vincent's Clinical School, University of NSW, Sydney, Australia.
3. Center of Medical Immunology, Institute for Research in Biomedicine, Faculty of Biomedical Sciences, University of the Italian Switzerland (USI), Bellinzona, Switzerland.
4. Pediatric Respiratory Diseases Research Center, National Research Institute of Tuberculosis and Lung Diseases (NRITLD), Shahid Beheshti University of Medical Sciences, Tehran, Iran.
5. Department of Pediatric Immunology, Dr. Sami Ulus Maternity and Children's Health and Diseases Training and Research Hospital, Ankara, Turkey.
6. Immunology Division, Walter and Eliza Hall Institute of Medical Research, Parkville, Victoria, Australia.
7. Department of Medical Biology, University of Melbourne, Parkville, Victoria, Australia.
8. Department of Clinical Immunology and Allergy, Royal Melbourne Hospital, Parkville, Victoria, Australia.
9. Laboratory of Human Genetics of Infectious Diseases, Necker Branch, INSERM U1163, Necker Hospital for Sick Children, Paris, France, EU.
10. Paris Descartes University, Imagine Institute, Paris, France, EU.
11. Innate Immunity Unit, Pasteur Institute, Inserm U1223, Paris, France, EU.
12. The Charles Bronfman Institute for Personalized Medicine, and the Department of Genetics and Genomic Sciences, Icahn School of Medicine at Mount Sinai, New York, NY, USA.
13. Human Evolutionary Genetics Unit, Department of Genomes and Genetics, Pasteur

Institute, Paris, France, EU.
14. Centre National de la Recherche Scientifique, UMR 2000, Paris, France, EU.
15. Center of Bioinformatics, Biostatistics and Integrative Biology, Pasteur Institute, Paris, France, EU.
16. Department of Pediatrics, Hiroshima University Graduate School of Biomedical & Health Sciences, Hiroshima, Japan.
17. Institute for Clinical and Molecular Virology, University Erlangen-Nuremberg, Germany, EU.
18. Department of Pediatric Immunology and Allergy, Ankara University School of Medicine, Ankara, Turkey.
19. Department of Pediatric Infectious Diseases, Dr. Sami Ulus Maternity and Children's Health and Diseases Training and Research Hospital, Ankara, Turkey.
20. Immunology Program, Memorial Sloan Kettering Cancer Center, New York, NY, USA.
21. Weill Cornell Graduate School of Medical Sciences, New York, NY, USA.
22. Centre for Molecular and Cellular Biology of Inflammation, King's College London, London, UK.
23. Department of Vaccine Discovery, La Jolla Institute for Allergy and Immunology, La Jolla, CA, USA.
24. University of California San Diego, Department of Medicine, La Jolla, CA, USA.
25. EA4340 and Pathology Department, Ambroise Paré Hospital AP-HP, Versailles Saint-Quentin-en-Yvelines University, Paris-Saclay University, Boulogne, France, EU.
26. Department of Infectious Diseases, Leiden University Medical Center, Leiden, The Netherlands, EU.
27. Study Center of Immunodeficiencies, Necker Hospital for Sick Children, AP-HP, Paris, France, EU.
28. Institute of Microbiology, ETH Zurich, Switzerland.
29. Howard Hughes Medical Institute, New York, USA.
30. Pediatric Hematology-Immunology Unit, Necker Hospital for Sick Children AP-HP, Paris, France, EU.

#, b,* Equal contributions
a Current address: The W. Harry Feinstone Department of Molecular Microbiology and Immunology, The Johns Hopkins Bloomberg School of Public Health, Baltimore, MD, USA.
@ Correspondence: rmartinezb@rockefeller.edu
jean-laurent.casanova@rockefeller.edu

Abstract

Hundreds of patients with autosomal recessive, complete IL-12p40 or IL-12Rβ1 deficiency have been diagnosed over the last 20 years. They typically suffer from invasive mycobacteriosis and, occasionally, from mucocutaneous candidiasis. Susceptibility to these infections is thought to be due to impairments of IL-12-dependent IFN-γ immunity, and IL-23-dependent IL-17A/IL-17F immunity, respectively. We report here patients with autosomal recessive, complete IL-12Rβ2 or IL-23R deficiency, lacking responses to IL-12 or IL-23 only, all of whom, surprisingly, display mycobacteriosis without candidiasis. We show that αβ T, γδ T, B, NK, ILC1, and ILC2 cells from healthy donors preferentially produce IFN-γ in response to IL-12, whereas NKT, MAIT, and ILC3 cells preferentially produce IFN-γ in response to IL-23. We also show that the development of IFN-γ-producing $CD4^+$ T cells, including, in particular, mycobacterium-specific Th1* cells ($CD45RA^-CCR6^+$), is dependent on both IL-12 and IL-23. Finally, we show that *IL12RB1*, *IL12RB2*, and *IL23R* have similar frequencies of deleterious variants in the general population. The comparative rarity of symptomatic patients with IL-12Rβ2 or IL-23R deficiency, relative to IL-12Rβ1 deficiency, is, therefore, due to lower clinical penetrance. These experiments of Nature show that human IL-12 and IL-23 are both crucial for IFN-γ-dependent immunity to mycobacteria, both individually and much more so cooperatively.

Introduction

Life-threatening infectious diseases during the course of infection in otherwise healthy individuals can result from single-gene inborn errors of immunity (*1*, *2*). Mendelian susceptibility to mycobacterial disease (MSMD) is characterized by severe disease upon exposure to weakly virulent mycobacteria, such as *Mycobacterium bovis*-Bacille Calmette-Guérin (BCG) vaccines and environmental mycobacteria (*3*, *4*). Affected patients are also at risk of severe infections with *M. tuberculosis, Salmonella*, and, more rarely, other intramacrophagic bacteria, fungi, and parasites (*4*). All known genetic etiologies of MSMD affect IFN-γ-mediated immunity (*4*, *5*).

The most common etiology is autosomal recessive (AR) IL-12Rβ1 deficiency, which has been reported in over 200 kindreds since 1998 and has probably been diagnosed in many more (*4*, *6–9*). IL-12Rβ1 deficiency displays incomplete clinical penetrance for MSMD, and can also underlie monogenic tuberculosis in families with no history of infection with environmental mycobacteria or BCG (*4*, *7*, *10*). IL-12Rβ1 dimerizes with IL-12Rβ2 to form the IL-12 receptor (*11*), or with IL-23R to form the IL-23 receptor (*12*). *IL12B* encodes the p40 subunit common to both IL-12 (with p35) and IL-23 (with p19) (*13*). Consistently, AR IL12p40 deficiency, which has been reported in over 50 kindreds, is a clinical phenocopy of IL-12Rβ1 deficiency (*4*, *14*).

Both IL-12 immunity and IL-23 immunity are abolished in these two disorders. Unlike other etiologies of MSMD, these two disorders can also underlie chronic mucocutaneous candidiasis (CMC), which is seen in about 25% of patients, due to impaired IL-17A/IL-17F-mediated immunity (*6*, *15–17*). Indeed, all known genetic etiologies of isolated or syndromic CMC affect IL-17A/IL-17F (*16*, *18–22*). Studies of mouse models

have suggested that disruption of the IL-12-IFN-γ circuit, particularly in $CD4^+$ helper T cells (Th1), underlies mycobacteriosis in these patients, whereas disruption of the IL-23-IL-17 circuit, particularly in Th17 cells, underlies candidiasis (*13*). However, the respective contributions of human IL-12 and IL-23 to IFN-γ-dependent MSMD and IL-17A/F-dependent CMC have remained elusive in the absence of inborn errors of IL-12p35, IL-12Rβ2, IL-23p19, or IL-23R.

Results

Homozygous *IL12RB2* and *IL23R* variants in two MSMD kindreds

We searched for rare, biallelic, non-synonymous and splice variants of *IL12A*, *IL12RB2*, *IL23A*, and *IL23R,* by whole-exome sequencing (WES) in patients with unexplained MSMD only (*n*=555), CMC only (*n*=214), or both MSMD and CMC (*n*=27). We identified two MSMD kindreds with mutations of *IL12RB2* or *IL23R*. Kindred A (Fig 1A) is a consanguineous Turkish family, the proband of which (P1; 7.6% homozygosity; Fig 1A) had MSMD (Case Reports, SOM, Fig. S1A). Kindred B (Fig. 1B) is a consanguineous Iranian family with two MSMD-affected children (P4 and P5; 3.5% of homozygosity for P5, Fig. 1B, Fig. S1B-D). These two kindreds were analyzed independently, by a combination of WES and genome-wide linkage (GWL) analysis (Fig. S1E, F). In kindred A, the c.412C>T mutation of *IL12RB2* results in a premature stop codon (Q138X) upstream from the segment encoding the transmembrane domain of IL-12Rβ2 (Fig. 1C). In kindred B, the c.344G>A mutation of *IL23R* results in the C115Y substitution, at a key residue in the extracellular domain of IL-23R (*23*) (Fig. 1D). The *IL12RB2* and *IL23R* loci are located in tandem on chromosome 1, and within the largest MSMD-linked

chromosomal regions in kindreds A and B, respectively (Fig. S1E-G). The three MSMD patients are homozygous for the mutant alleles (Fig. 1A-B, Fig. S1H-I). Incomplete clinical penetrance for MSMD was observed in kindred A, as *IL12RB2*-homozygous and BCG-vaccinated individual II.3 (P2; 9.1% of homozygosity) had tuberculosis but not MSMD, and II.4 (P3; 10.8% of homozygosity) had neither (Case Reports, SOM). None of the five homozygous mutant individuals from kindreds A (P1-P3) and B (P4-P5) had ever displayed signs of CMC. Principal component analysis (PCA) based on WES data confirmed the ancestries of these patients (Fig S1J) (*24*). The *IL12RB2* Q138X mutation was reported in the heterozygous state in two of 123,098 individuals in the gnomAD database (http://gnomad.broadinstitute.org), whereas the *IL23R* C115Y mutation was not reported in any of the 122,998 individuals sequenced at this site. These mutations were not found in a cohort of 3,869 individuals of Middle Eastern descent with neurological diseases (data not shown). Finally, both variants have CADD scores well above their respective MSCs (*25*, *26*). These data suggested that MSMD patients from kindreds A and B had AR deficiencies of IL-12Rβ2 and IL-23R, respectively, the former disorder displaying incomplete penetrance for MSMD.

The *IL12RB2* and *IL23R* mutant alleles are loss-of-function

We assessed the expression and function of these mutant alleles, by using retrovirus-mediated gene transfer to express C-terminal V5-tagged wild-type (WT) or mutant IL-12Rβ2 or IL-23R proteins in a B-lymphocyte cell line (LCL) that expressed STAT3 and IL-12Rβ1 and was engineered to express $STAT4^{IRES\text{-}GFP}$ in a stable manner (referred to here as LCL-B^{STAT4} cells) (*27*). The *IL12RB2* Q138X mutation resulted in

abundant IL-12Rβ2 mRNA production (Fig. S1K), but the corresponding protein was undetectable (Fig. 1E, Fig. S1L). The *IL23R* C115Y mutation did not alter the amount of mRNA (Fig. S1K) or protein detected (Fig. 1F, Fig. S1L). However, the mutant IL-23R protein did not undergo normal *N*-glycosylation (Fig. 1F) and was much less abundant on the cell surface than the exogenous WT protein (Fig. 1G, Fig. S1M). Next, we stimulated the LCL-B^{STAT4} cells expressing either the WT or mutant IL-12Rβ2 and IL-23R proteins with IL-12, IL-23, or IFN-α as a positive control. Human IL-12-dependent signaling via IL-12Rβ1/IL-12Rβ2 results in STAT4 activation, whereas IL-23-dependent signaling via IL-12Rβ1/IL-23R preferentially results in STAT3 activation, although STAT4 may also be activated (*13*). LCL-B^{STAT4} cells expressing WT, but not mutant IL-12Rβ2, displayed STAT4 phosphorylation in response to IL-12 (Fig. 1H). Similarly, the expression of WT IL-23R, but not mutant IL-23R, conferred responsiveness to IL-23, as assessed by the level of phosphorylation of STAT3 (Fig. 1I) and STAT4 (Fig. S2A) and their upstream Janus kinases TYK2 and JAK2 (Fig. S2B). Cells expressing WT, but not mutant IL-12Rβ2 or IL-23R, also produced CXCL10 in response to IL-12 or IL-23 stimulation, respectively (Fig. S2C). Pretreatment of the cells with kifunensine, an inhibitor of glycosylation that can rescue mild misfolding and gain-of-glycosylation mutants (*28*), did not restore the function of IL-23R C115Y, suggesting that the mutation is severely deleterious (Fig. S2D). Thus, the Q138X *IL12RB2* and C115Y *IL23R* mutant alleles are completely loss-of-function (LOF) for the IL-12 and IL-23 signaling pathways, respectively, at least in these experimental conditions. These experiments demonstrated the role of each mutant allele cDNA over-expressed in isolation. Our next set of experiments used patient-derived cells, which capture the effects of the patients' full genotypes at these loci in the context of their

own genome.

Autosomal recessive IL-12Rβ2 and IL-23R complete deficiencies

We assessed the expression and function of IL-12Rβ2 and IL-23R in patient-derived cell lines. *Herpesvirus saimiri*-transformed T (HVS-T) cells from a healthy control, P1 (IL-12Rβ2 Q138X), and an IL-12Rβ1-deficient patient (*4*) were left unstimulated, or stimulated with IL-12 or IFN-α. The healthy control cell line, but not cells from P1 or the IL-12Rβ1-deficient patient, displayed STAT4 phosphorylation in response to IL-12 (Fig. 1J). This defect was confirmed in HVS-T cells from P2 and P3 (Fig. S2E). Furthermore, the retroviral transduction of P1 cells with WT *IL12RB2* restored STAT4 phosphorylation in response to IL-12, whereas retrovirus-mediated transduction with an empty vector did not (Fig. 1J). In parallel, EBV-B cells from a healthy control, P4 (IL-23R C115Y), and an IL-12Rβ1-deficient patient were left unstimulated, or were stimulated with IL-23 or IFN-α. Control EBV-B cells responded to IL-23 by phosphorylating STAT3, whereas cells from P4 and the IL-12Rβ1-deficient patient did not (Fig. 1K). The transduction of EBV-B cells from P4 with WT *IL23R* rescued both the weak IL-23R expression on the surface of P4 EBV-B cells (Fig. S2F-G), and the defective IL-23 response (Fig. 1K, Fig S2H), whereas retrovirus-mediated transduction with an empty vector did not. IL-12Rβ1- and TYK2-deficient cells were used as negative controls for the IL-23- and IFN-α-dependent phosphorylation of STAT3, respectively (Fig. S2H). The IL-23 response was not restored by the prior treatment of EBV-B cells from P4 with kifunensine (Fig. S2I-J). Thus, the patients from kindreds A and B had complete forms of AR IL-12Rβ2 deficiency and AR IL-23R deficiency, respectively.

IL12RB1, *IL12RB2*, and *IL23R* have not evolved under purifying selection

The much smaller number of biallelic mutations responsible for MSMD found in *IL12RB2* and *IL23R* than in *IL12RB1* suggested that *IL12RB2* and *IL23R* might have evolved under stronger selective constraints, preventing the accumulation of monoallelic deleterious variants. We tested this hypothesis by estimating the levels of purifying selection acting on all human genes with a generalized linear mixed model approach, comparing protein-coding polymorphisms and divergence data (*29*). Exome data from the 1,000 Genomes project (*30*) were aligned with the chimpanzee reference genome, yielding exploitable data for a total of 18,969 protein-coding genes (Methods, SOM). The proportion of non-deleterious amino-acid variants (f) was estimated at 46.7% for *IL12RB1* [95% confidence interval: 30.4%–71.7%], 61.7% for *IL12RB2* [95%CI: 42.1%–90.3%], and 49.0% for *IL23R* [95%CI: 31.1%–77.4%] (Table S1). These three genes were among the 50% least constrained genes, and their high levels of amino acid-altering polymorphisms, relative to divergence, were consistent with the action of weak negative selection (as shown by the negative estimates for the population selection coefficient γ), as observed for most human protein-coding genes. Moreover, the neutrality index (NI) and gene damage index (GDI, (*31*)) of *IL12RB1*, *IL12RB2,* and *IL23R* were intermediate (Fig. 2A-B). The results were similar when looking at alternative parameters of selection such as RVIS (*32*) and *f* (*33*) (data not shown). Consistently, numerous missense and predicted LOF variants of *IL12RB1*, *IL12RB2,* and *IL23R* are present, in the heterozygous state, in gnomAD (Fig. S3A-C). There are also fewer homozygous missense variants for these three genes (Fig. 2C-D, Fig. S3D). Overall, this computational study suggested that neither

IL12RB2 nor *IL23R* had evolved under purifying selection, or even under strong negative selection, and that they were no less mutated than *IL12RB1* in the general population. These findings support the alternative hypothesis that the paucity of MSMD patients with IL-12Rβ2 or IL-23R deficiency, relative to the number of patients identified with IL-12Rβ1 deficiency, results from lower clinical penetrance for MSMD.

Null mutations in *IL12RB1*, *IL12RB2* and *IL23R* are rare

We tested these computational predictions through experimental determinations of the actual frequency of *IL12RB2* and *IL23R* LOF mutations in the general population, by using the same retroviral system to express all previously untested variants of both genes present in the homozygous state in gnomAD (Fig. 2C-D, Fig. S3E-F), in LCL-B^{STAT4} cells. All homozygous *IL12RB1* variants present in the general population that have been tested (6 of 16) have been shown to be neutral (*34*). We stimulated the LCL-B^{STAT4} cells expressing either the WT or homozygous gnomAD variants of IL-12Rβ2 (15 variants) and IL-23R (13 variants) proteins with IL-12, IL-23, or IFN-α as a positive control. The *IL12RB2* mutation L130S encoded a protein that was expressed (Fig. S3G) but not functional (Fig. 2E). The L130S mutation of *IL12RB2* was found to be present in the homozygous state in 1 of 123,092 individuals in the gnomAD database. The *IL12RB2* K649N mutation affects a splice site, and may, therefore, cause a missense or splicing mutation, resulting in the deletion of exon 15 (Δex15) (Fig S3H-I). The *IL12RB2* K649N mutation was found to encode a protein that was both expressed (Fig. S3G) and functional (Fig. 2E), like the WT protein, whereas the *IL12RB2* Δex15 mutation encoded a protein with a lower molecular weight (Fig. S3G) that was non-functional (Fig. 2E). The *IL12RB2*

K649N mutation was identified in 1 of 138,539 individuals in the gnomAD database. None of the *IL23R* mutations tested resulted in a complete loss of protein expression or function (Fig. S3J, Fig. 2F). These and previous data (*34*) suggest that homozygous complete LOF mutations of *IL12RB2*, *IL23R* and *IL12RB1* occur in the general population at a frequency of <1 in 100,000 individuals. This frequency is similar to that of autosomal recessive IL-12Rβ1 deficiency, the penetrance of which for MSMD reaches a plateau of about 80% in adults (*6*, *7*).

In vivo Th development in IL-12Rβ2 and IL-23R deficiency

As a first approach to testing the hypothesis that IL-12Rβ2 and IL-23R deficiencies have a lower clinical penetrance for MSMD than IL-12Rβ1 deficiency, we set out to decipher the cellular basis of MSMD in patients with these disorders. In humans and mice, IL-12 and IL-23 are thought to promote mutually exclusive $CD4^+$ T-helper cell fates (*13*). Before testing for IL-12- and IL-23-dependent effects on the differentiation of human Th cells, we compared the frequencies of leukocyte subsets in healthy controls, an *IL12RB2* Q138X patient, an *IL23R* C115Y patient, and at least one IL-12Rβ1-deficient patient. The frequencies of innate lymphoid cells (ILCs), B, NK, γδ T, total T ($CD3^+$), $CD4^+$ αβ T, $CD8^+$ αβ T, T_{reg}, and T_{FH} cells were normal in patients of all genotypes (Fig. S4A). Patients with IL-12Rβ2-, IL-23R-, or IL-12Rβ1-deficiency had a low frequency of MAIT cells (Fig. S4A), consistent with previous findings for IL-12Rβ1- and STAT3-deficient patients (*35*). The frequency of naïve cells in the $CD4^+$ and $CD8^+$ T-cell populations was higher, and that of memory cells was lower in IL-12Rβ2-, IL-23R-, and IL-12Rβ1-deficient patients than in healthy controls (Fig. 3A, left panel, Fig. S4B-C). IL-12Rβ2-, IL-23R-, and IL-12Rβ1-

deficient patients had lower frequencies of memory Th1 ($CXCR3^+CCR6^-$) and Th1* ($CXCR3^+CCR6^+$) cells than healthy controls, IL-12Rβ1-deficient patients also had lower frequencies of Th17 ($CCR4^+CCR6^+$) cells, and the frequency of Th2 ($CCR4^+CCR6^-$) cells was similar in patients of all genotypes (Fig. 3A, right panel). However, within the $CD4^+$ memory compartment, the percentages of Th1* and Th17 cells were low in some IL-12Rβ1-deficient patients, but not in IL-12Rβ2- or IL-23R-deficient patients, whereas Th1 and Th2 percentages were normal in patients of all genotypes (Fig. S4D). These surprising findings suggested that isolated deficiencies of IL-12 or IL-23 responses had similar and slightly milder consequences, in terms of Th1, Th1*, and perhaps Th17 development, than a combined deficiency.

In vitro Th differentiation in IL-12Rβ2 and IL-23R deficiency

We then investigated the effects of IL-12 and IL-23 signaling defects on the generation of $CD4^+$ T-cell subsets upon stimulation with polarizing cytokines *in vitro*. Naïve ($CD45RA^+CCR7^+$) $CD4^+$ T cells from healthy donors, IL-12Rβ2-, IL-23R-, and IL-12Rβ1-deficient patients were purified and cultured under Th0 (non-polarizing) or "Th1"-, "Th2"- or "Th17"-polarizing conditions (*36*), and the production of various cytokines was measured in culture supernatants with cytometric bead arrays or by ELISA. "Th1" differentiation *in vitro*, which occurs in the presence of IL-12 and is assessed by monitoring IFN-γ production, was abolished in cells from IL-12Rβ2- and IL-12Rβ1-deficient patients, but intact in IL-23R-deficient patient cells (Fig. 3B). By contrast, "Th17" differentiation *in vitro* in the presence of IL-23, as assessed by monitoring IL-17F production, was maintained in IL-12Rβ2-deficient cells, but abolished in naïve $CD4^+$ T cells from IL-23R-

and IL-12Rβ1-deficient patients (Fig. 3B). Following "Th2" differentiation *in vitro*, which occurs in the presence of IL-4, cells of all genotypes produced similar amounts of IL-10 (Fig. 3B). Collectively, these data suggest that the cytokine-dependent *in vitro* differentiation of naïve $CD4^+$ T cells into "Th1" and "Th17" cells is affected by IL-12Rβ2 deficiency and IL-23R deficiency, respectively, consistent with previous findings (*13*). We probed genotype-dependent effects on the generation of cytokine-producing $CD4^+$ T cells *in vivo* further, by purifying naïve ($CD45RA^+CCR7^+$) and memory ($CD45RA^-$) $CD4^+$ T cells from healthy donors, IL-12Rβ2-, IL23R- or IL-12Rβ1-deficient patients and culturing them with polyclonal TCR-activating ligands (Th0 conditions) (*36*). As expected, IL-12Rβ1- and IL23R-deficient cell cultures displayed only low levels of IL-17A and IL-17F production (Fig. 3C). Similar amounts of IL-10 were again produced by all cells tested. Surprisingly, the production of IFN-γ, TNF, and IL-2 by memory $CD4^+$ T cells was reduced not only by IL-12Rβ1 or IL-12Rβ2 deficiency, but also by IL-23R deficiency, possibly due to T cell-intrinsic functional defects or to the low frequency of Th1 and/or Th1* cells in the three groups of patients.

***Mycobacterium*-specific IFN-γ production is compromised in Th cells**

We assessed the potential effects of deficiencies of IL-12Rβ1, IL-12Rβ2, or IL-23R on the induction of *Mycobacterium*-specific $CD4^+$ T-cell responses *in vivo*, by analyzing memory $CD4^+$ T cells from healthy controls and patients of each genotype (*37*). Both BCG-vaccinated and -unvaccinated individuals have been shown to robustly produce IFN-γ in response to BCG (*38*) and mycobacteria-derived antigens (*39*). Multiple T-cell lines were generated from sorted $CD4^+CD45RA^-CCR6^-$ cells (containing Th1 and Th2 cells and known to be enriched in viral antigen-reactive T cells) and $CD4^+CD45RA^-CCR6^+$ cells

(containing Th1* and Th17 cells known to be enriched in bacterial and fungal antigen-reactive T cells, respectively) separately (*40*). Following polyclonal stimulation, both $CCR6^+$ and $CCR6^-$ T cells produced IFN-γ in similar amounts for healthy controls and all patients (Fig. S5A). By contrast, IL-17A and IL-22 were produced mostly by $CCR6^+$ cells for healthy controls and an IL-12Rβ2-deficient patient, but not for IL-12Rβ1- and IL-23R-deficient patients (Fig. S5A), consistent with the notion that IL-23 is an important inducer of the production of IL-17A and IL-22 by $CD4^+$ T cells (*41*). In the same experiment, the production of IL-4 was not affected by any of the mutations tested (Fig. S5A). All T-cell lines were then screened *in vitro* for recall responses to influenza virus, respiratory syncytial virus (RSV), BCG, and *Mycobacterium tuberculosis* (MTB). Several T-cell lines from both healthy donors and patients proliferated in response to the antigens tested (Fig. S5B). As expected, the frequency of influenza- and RSV-reactive cells was higher in $CCR6^-$ T-cell lines, whereas the frequency of BCG- and MTB-reactive cells was higher in $CCR6^+$ T-cell lines. (Fig. S5B-C). No major differences in the frequency of precursor cells specific for the tested antigens (Fig. S5C) were observed, but genotype-dependent defects were observed in the production of cytokines by proliferating T cells. The production of IFN-γ, but not of IL-4, by influenza virus- or RSV-reactive $CCR6^-$ T cells was impaired in IL-12Rβ2- and IL-12Rβ1-deficient patients, but not in IL-23R-deficient patients (Fig. S5D). Interestingly, the levels of IFN-γ production by BCG- and MTB-responding $CCR6^+$ T cells were low in IL-12Rβ1-, IL-12Rβ2-, and IL-23R-deficient patients (Fig. 4A, left panels). IL-17A was produced by only a few healthy donor $CCR6^+$ T cells in response to BCG and MTB, precluding comparisons between genotypes (Fig. 4A). In the same cells, IL-22 production was low in IL-12β1- and IL-23R-deficient patients, but not in IL-12Rβ2-

deficient patients (Fig 4A), providing further evidence of a functional IL-23R deficiency. However, the role of human IL-22 in immunity to infection remains undetermined. Interestingly, $CD4^+$ T cells from *Il23a-/-* mice showed severely defective IL-17 and IL-22 production, mildly reduced IFN-γ production, and increased mycobacterial growth, when compared with WT mice following *M. tuberculosis* infection (*42*). Yet, *Il17ra-/-* and *Il22-/-* mice did not differ from WT mice in their control of *M. tuberculosis* growth (*42*), unlike *Ifng-/-* mice (*43*) suggesting that IL-23-dependent IFN-γ production is involved in this setting. Other studies have shown that IL-23 augments local IFN-γ production in the lung and limits pulmonary *M. tuberculosis* replication in mice (*44*). Overall, these data indicate that, in the absence of either IL-12 or IL-23 signaling, *Mycobacterium*-specific IFN-γ production is compromised in $CCR6^+$ memory $CD4^+$ Th1* cells, a cellular phenotype common to inherited ROR-γ/ROR-γT (*36*) and SPPL2A deficiencies (Kong X-F., Martinez-Barricarte R., *Nature Immunology*, in press).

Lymphocyte subsets respond differently to IL-12 and IL-23

However, the mycobacterial disease in the patients studied cannot be entirely dependent on impaired effector functions of $CD4^+$ T cells alone, as patients with HLA-II deficiency due to mutations of *CIITA*, *RFXANK*, *RFXAP*, or *RFX5,* with very low frequencies of functional $CD4^+$ αβ T cells, are not prone to clinical disease caused by weakly virulent mycobacteria (*45*). Indeed, BCG or environmental mycobacterial disease of genetic origin in patients without isolated or syndromic MSMD, has been documented only in patients with severe combined immunodeficiency (SCID), who lack all types of

endogenous T cells (*46*). An additional lack of NK cells in SCID patients seems to underlie more frequent and severe forms of mycobacterial disease (unpublished), although isolated NK deficiency does not confer a predisposition to mycobacterial disease (*47–49*). We therefore assessed mRNA levels for *IL12RB1*, *IL12RB2*, and *IL23R* in various leukocyte subsets, and assessed the consequences of IL-12 and IL-23 signaling in each of these cell types. Human *IL12RB1* mRNA production has been reported in many types of human leukocytes, the lowest levels being reported in B cells and monocytes and the highest levels in NK cells (*50*). *IL12RB2* and *IL23R* display a high degree of sequence identity and probably arose through gene duplication (*12*), but they nevertheless have different patterns of expression, with *IL12RB2* mRNA levels highest in γδ T cells and NK cells, whereas *IL23R* mRNA levels are highest in γδ T cells and only moderate in $CD4^+$ and $CD8^+$ αβ T cells (*50*). We confirmed these findings (Fig. S6A), and stimulated purified B, $CD4^+$ αβ T, $CD8^+$ αβ T, γδ T, and NK cells from healthy donors with IL-12 or IL-23 for 6 h, before assessing the genome-wide transcriptional consequences by mRNA microarray analysis. Cytokine-specific and cell type-specific patterns were observed (Tables S2 and S3). Strikingly, *IFNG* transcripts were the most consistently induced across cell types and stimuli (Fig. 4C-D). This result was validated by qPCR (Fig 4E) and ELISA for IFN-γ on cell culture supernatants (Fig. 4F). We expanded this study to include MAIT, NKT cells, and ILCs, all of which have been reported to be potent IFN-γ producers (reviewed in (*51*, *52*)). MAIT and NKT cells clearly responded to each cytokine by producing IFN-γ, but they responded more strongly to IL-23 (Fig. 4G-H). ILC1 and ILC2 isolated from peripheral blood responded to IL-12, but not IL-23, by producing IFN-γ (Fig. 4H). ILC3 isolated from tonsillar tissue clearly responded to IL-23 and IL-12 by producing IFN-γ

(Fig. 4I). Finally, the stimulation of PBMCs from healthy donors or IL-12Rβ1-deficient patients with *M. bovis* BCG together with IL-12 or IL-23 revealed that IL-12 strongly potentiated the IFN-γ response to BCG, but that IL-23 also increased IFN-γ production, albeit to a lesser extent (Fig. S6B-D).

Discussion

Collectively, these data shed light on the respective contributions of IL-12 and IL-23 to human immunity to *Mycobacterium* and *Candida*, through the discovery and characterization of AR complete IL-12Rβ2 and IL-23R deficiencies in two multiplex MSMD kindreds without CMC. The surprising absence of CMC in IL-23R-deficient P4 and P5, as in most patients with complete IL-12Rβ1 deficiency, may be due to the incomplete penetrance of IL-23 deficiency for poor IL-17A/IL-17F production, or the incomplete penetrance of low levels of IL-17 production for CMC, or both. Indeed, all known forms of isolated or syndromic CMC disrupt IL-17A/F immunity (*16*, *18–22*). These data also reveal the specific transcriptional consequences of IL-12 vs. IL-23 signaling in human B, $CD4^+$ αβ T, $CD8^+$ αβ T, γδ T, MAIT, NKT, NK cells and ILCs, with a notable convergence on IFN-γ induction (Table S4). Clinically, these results add *IL12RB2* and *IL23R* to the list of 11 other genes (*IFNGR1, IFNGR2, STAT1, IL12B, IL12RB1, NEMO, CYBB, IRF8, ISG15, TYK2, SPPL2A*) mutated in MSMD patients, the products of which are all involved in IFN-γ-mediated immunity (*4*, *5*, *36*). Importantly, patients with deleterious mutations in IL17F, IL17RA, IL17RA, or ACT1 have CMC without mycobacterial disease immunity (*16*, *18–22*). Ouresults therefore reveal that both IL-12- and IL-23-dependent signaling pathways play critical roles in human anti-

mycobacterial immunity, via the induction of IFN-γ. Indeed, our findings show that human IL-12 and IL-23 are partly, but not totally redundant with each other, for IFN-γ-dependent anti-mycobacterial immunity. These findings in natural conditions in humans corroborate and extend previous experiments performed in mice (*42*).

IL-12- and IL-23-dependent induction of IFN-γ may occur either within the same cell type, or differentially across different cell types, and IL-23 may provoke IFN-γ by direct or indirect means (which may include IL-17- and IL-22-dependent and -independent processes). The absence of response to both these molecules, as in patients with complete IL-12Rβ1 deficiency, underlies MSMD with incomplete but high penetrance, reaching an estimated 65% by five years of age and 80% in adults (*4*). It was not possible to calculate the penetrance of IL-12Rβ2 and IL-23 deficiencies, but the data from our population and family genetic studies strongly suggest that penetrance is much lower in both these deficiencies, accounting for the diagnosis of IL-12Rβ1 deficiency in a hundred times as many kindreds to date. This notion is strongly supported by our accompanying report that as many as 1/1,000 Europeans homozygous for *TYK2* P1104A have normal responses to IL-12, and impaired responses to IL-23, rendering them vulnerable to tuberculosis and, more rarely, to MSMD (Boisson-Dupuis S, Ramirez-Alejo N., *et al*.). The primary, essential function of both IL-12 and IL-23 in humans is to induce IFN-γ and control mycobacteria and other intramacrophagic pathogens, perhaps due to the duplication of the loci encoding both these cytokines and their receptors. The contribution of IL-23 to IL-17 anti-fungal immunity is more modest and may be more recent in terms of evolution, as both the IL-23R-deficient patients described here, and most IL-12Rβ1-deficient patients described to date are not susceptible to *Candida*.

Acknowledgments

We thank the patients and their families for their collaboration, both branches of the Laboratory of Human Genetics of Infectious Diseases for helpful discussions and support, Y. Nemirovskaya, E. Anderson, M. Woolett, L. Amar and D. Papandrea for administrative support, and J. Gleeson (UCSD) for sharing WES data from individuals of middle eastern descent. The data presented in the manuscript are tabulated in the main paper and the Supplementary Online Materials. The WES data are available from the Sequence Read Archive (www.ncbi.nlm.nih.gov/sra) [accession numbers to be added when available]. The Laboratory of Human Genetics of Infectious Diseases is supported by grants from the National Institute of Allergy and Infectious Diseases (NIAID) grant numbers 5R37AI095983, R01AI089970 and K99AI127932, the National Center for Research Resources and the National Center for Advancing Sciences (NCATS) of the National Institutes of Health grant number UL1TR001866, The Rockefeller University, the St. Giles Foundation, the European Research Council (ERC-2010-AdG-268777 and grant no. 323183), *Institut National de la Santé et de la Recherche Médicale*, Paris Descartes University, the Integrative Biology of Emerging Infectious Diseases Laboratory of Excellence (ANR-10-LABX-62-IBEID) and by the French National Research Agency (ANR) under the "*Investissement d'avenir*" program (grant ANR-10-IAHU-01), ANR-TBPATHGEN (grant ANR-14-CE14-0007-01), ANR-IFNPHOX (grant ANR13-ISV3-0001-01), ANR-GENMSMD (grant ANR16-CE17-0005-01). This work was supported by NIAID award #U19AI118626 (to AS and FS). JM was funded by the Canadian Institutes of Health Research, The NIH Translational Science Award (CTSA) program (#UL1 TR000043), the Swiss National Science Foundation (grant n. IZKOZ3_173586), The

Charles H. Revson Foundation, and the NIAID (1K99AI127932-01A1). RMB was supported by the European Molecular Biology Organization (EMBO). NRA was supported by the National Council of Science and Technology of Mexico (CONACYT, 264011) and the Stony Wold-Herbert Fund Fellowship Grant. YI was supported by the AXA Research Fund. SGT, EKD and CSM are supported by research grants and fellowships from the National Health and Medical Research Council of Australia (SGT, CSM, EKD) and the Office of Health and Medical Research of the State Government of NSW Australia (CSM). AS is supported by NIH research grant HHSN272200900044C. JB is supported by SRC2017. The Institute for Research in Biomedicine and F.S. are supported by the Helmut Horten Foundation.

Figure legends

Figure 1: Identification of homozygous complete loss-of-function IL-12Rβ2 Q138X and IL-23R C115Y mutations in families with MSMD.

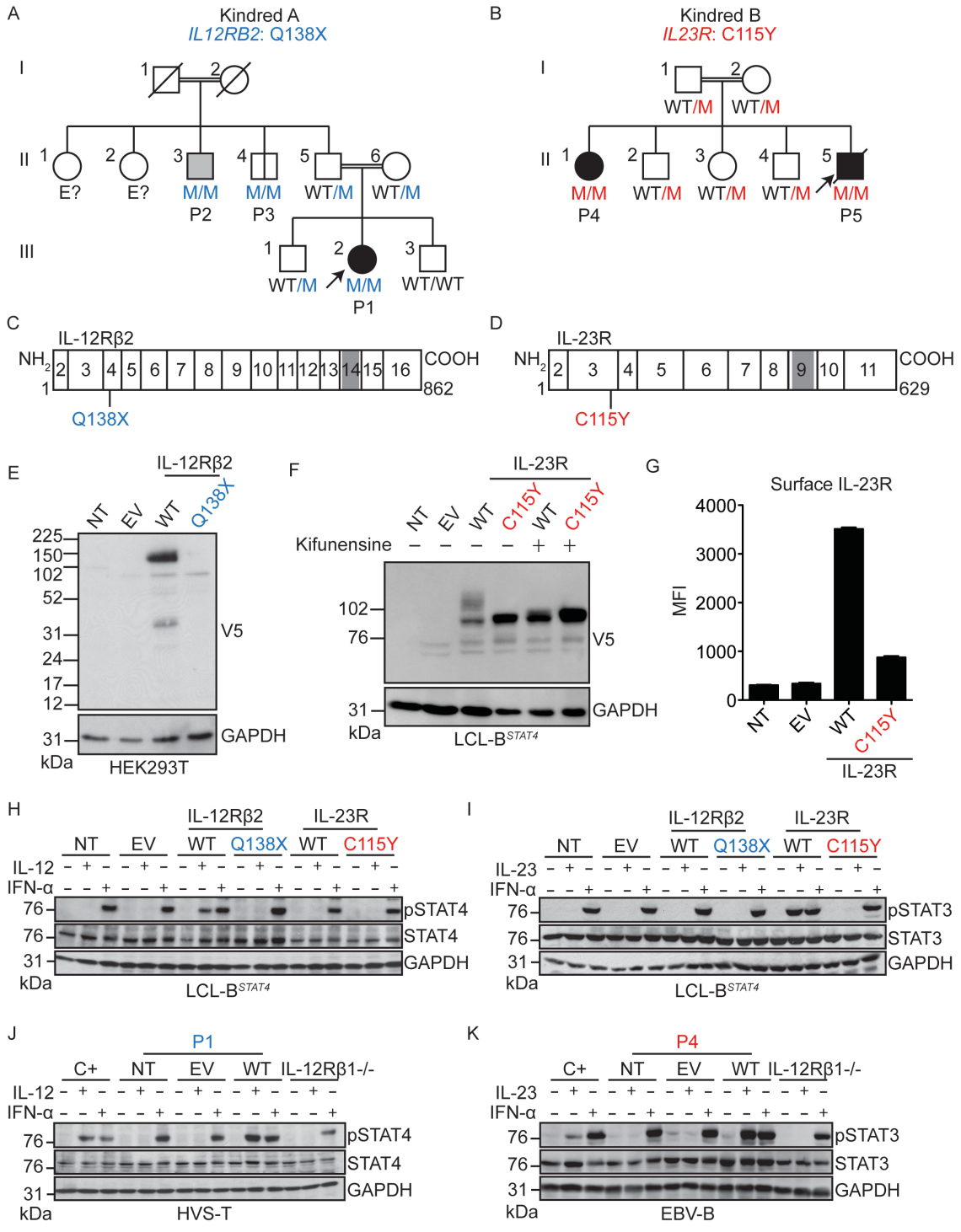

A, B) Pedigrees of the two kindreds studied in this report. The gene and mutation are indicated under the kindred name. Solid black symbols indicate patients with MSMD and solid gray symbols indicate cases of primary tuberculosis during childhood. Symbols linked with a double line indicate consanguinity. The genotype is indicated under each symbol, with M corresponding to the mutation found in each kindred. Arrows indicate the index case in each family. **C, D)** Schematic representation of IL-12Rβ2 (C) and IL-23R (D). Rectangles represent individual exons of the gene, with the exon numbers indicated within the rectangle. In each case, the N terminal portion of the protein is the extracellular domain, and gray shaded areas represent the transmembrane domain. The mutations studied here are indicated below each protein, in the corresponding exons. **E)** HEK293T cells were either non-transfected (NT) or transfected with an empty vector (EV), a vector containing the C-terminal V5-tagged WT or Q138X mutant versions *IL12RB2*. Western blotting was performed with antibodies against the V5 tag, or GAPDH as a loading control. **F)** LCL-B^{STAT4} cells were either non-transduced (NT), or transduced with retroviruses generated with an empty vector (EV) or with vectors containing the WT or C115Y mutant versions of *IL23R*. Cells were either left untreated, or treated with kifunensine to inhibit *N*-glycosylation. Western blotting was performed with antibodies against the V5 tag, or GAPDH as a loading control. **G)** LCL-B^{STAT4} cells from (F) were stained with an anti-IL-23R biotinylated primary antibody, then with avidin-PE, and the mean fluorescence intensity (MFI) for the PE signal was quantified by flow cytometry. **H)** LCL-B^{STAT4} cells were either left non-transduced (NT), or were transduced with retroviruses generated with an empty vector (EV) or vectors containing V5-tagged WT or Q138X mutant versions of *IL12RB2*, or WT or C115Y versions of *IL23R*. The cells were left unstimulated, or were

stimulated with IL-12 or IFN-α. Cell lysates were prepared, and western blotting was performed with antibodies against pSTAT4, total STAT4, and GAPDH. **I)** LCL-B^{STAT4} cells from (H) were left unstimulated, or were stimulated with IL-23 or IFN-α as a positive control. Cell lysates were prepared, and western blotting was performed with antibodies against pSTAT3, total STAT3, and GAPDH. **J)** HVS-T cells from a healthy control (C+), an IL-12Rβ1$^{-/-}$ patient or P1 (IL-12Rβ2 Q138X) were not transduced (NT), or were transduced with a retrovirus generated with an empty vector (EV) or a WT allele of *IL12RB2* and then stimulated with IL-12 or IFN-α. Western blotting was performed as described in (H). **K)** EBV-B cells from a healthy control (C+), an IL-12Rβ1$^{-/-}$ patient or P4 (IL-23R C115Y) were not transduced (NT), or were transduced with a retrovirus generated with an empty vector (EV) or a WT allele of *IL23R* and then stimulated with IL-23 or IFN-α. Western blotting was performed as described in (I).

Figure 2: *IL12RB2* and *IL23R* are evolving under weak purifying selection, and homozygous complete loss-of-function mutations of these genes occur rarely in the general population.

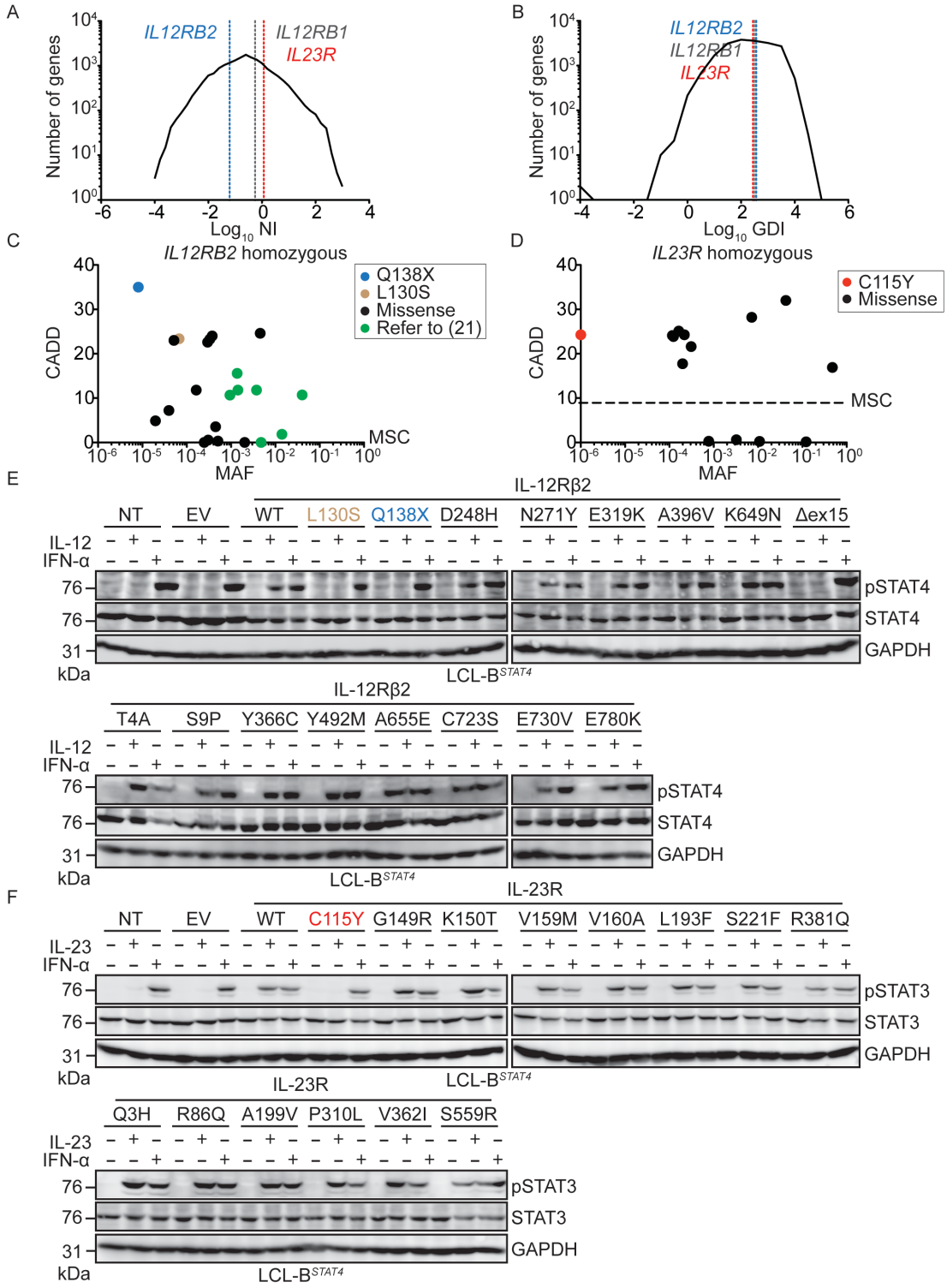

A, B) Graphic representation of all genes of the human genome according to the $\log_{10}$ of their (A) neutrality index (NI) or (B) gene damage index (GDI, (*31*)). *IL12RB2* (blue), *IL23R* (red), and *IL12RB1* (grey) are each indicated by a dashed vertical line. **C, D)** All homozygous variations found in gnomAD for *IL12RB2* (C) and *IL23R* (D) are plotted according to their CADD score (*y*-axis) and minor allele frequency (MAF, *x*-axis). The dashed line indicates the mutation significance cutoff (MSC, (*26*)) for each gene. **E)** LCL-B^{STAT4} cells were left non-transduced (NT), or were transduced with retroviruses generated with an empty vector (EV) or vectors containing V5-tagged WT or mutant versions of *IL12RB2*, including the 16 mutations indicated. These *IL12RB2* mutations are present in at least one individual in the gnomAD database. Cells were left unstimulated, or were stimulated with IL-12 or IFN-α. Cell lysates were prepared, and western blotting was performed with antibodies against pSTAT4, total STAT4, and GAPDH. **F)** LCL-B^{STAT4} cells were left non-transduced (NT), or were transduced with retroviruses generated with an empty vector (EV) or vectors containing V5-tagged WT or mutant versions of *IL23R*, for the 14 mutations indicated. With the exception of the C115Y mutation found in kindred B, these *IL23R* mutations are each present in at least one individual in the gnomAD database. Cells were left unstimulated, or were stimulated with IL-23 or IFN-α. Cell lysates were prepared, and western blotting was performed with antibodies against pSTAT3, total STAT3, and GAPDH.

Figure 3: Frequencies and responses of CD4$^+$ T cells from IL-12Rβ1-, IL-12Rβ2- and IL-23R-deficient individuals to polyclonal stimuli or Th-polarizing cytokines.

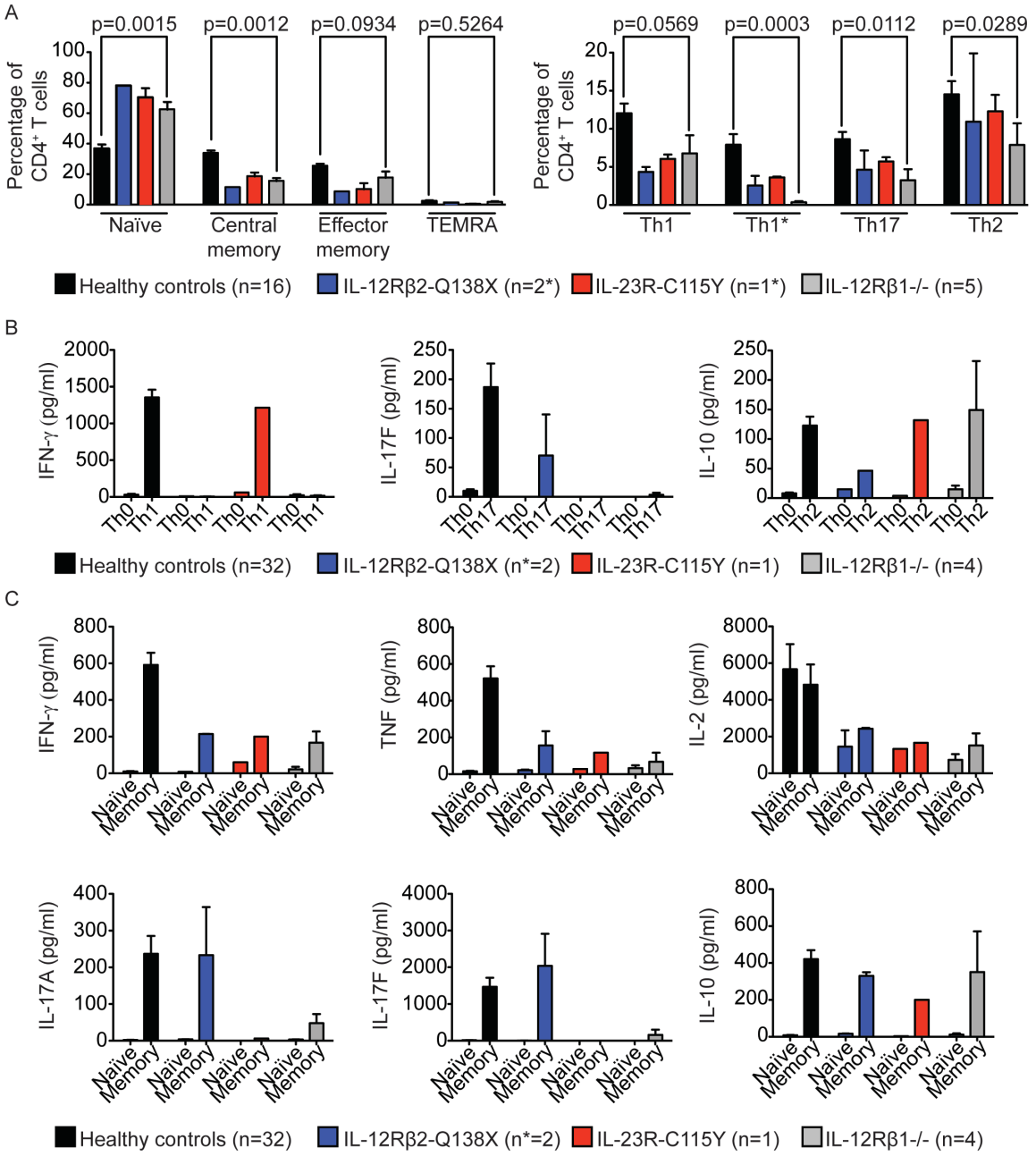

A) On the left, frequencies of naïve (CCR7$^+$CD45RA$^+$), central memory (CCR7$^+$CD45RA$^-$), effector memory (CCR7$^-$CD45RA$^-$) and T_{EMRA} (CCR7$^-$CD45RA$^+$) CD4$^+$CD3$^+$ T cells were measured in healthy controls (*n*=16), IL-12Rβ2-Q138X patients (*n*=2, one measured

twice), one IL-23R-C115Y patient (technical triplicates) and IL-12Rβ1$^{-/-}$ patients (*n*=5). The values shown are the percentage of total CD4^{+} T cells. On the right, frequencies of four subsets of CD4^{+} memory T cells (CD3^{+}CD45RA^{-}): Th1 (CCR6^{-}CCR4^{-}CXCR3^{+}), Th1* (CCR6^{+}CCR4^{-}CXCR3^{+}), Th17 (CCR6^{+}CCR4^{+}CXCR3^{-}) and Th2 (CCR6^{-} CCR4^{+}CXCR3^{-}) were measured in the same individuals as in the left panel. Error bars indicate the SEM. *P* values for the comparison of healthy controls with IL-12Rβ1-deficient patients in Mann-Whitney U-tests are shown. Formal statistical comparisons including IL-12Rβ2-Q138X and IL-23R-C115Y patients were not appropriate, due to the extremely small number of individuals (2 and 1, respectively). **B)** Naïve CD4^{+} T cells from healthy controls, two IL-12Rβ2-Q138X patients (P1 and P2), one IL-23R-C115Y patient (P4) and four IL-12Rβ1-deficient patients were either left unpolarized (Th0) or were polarized under Th1 conditions (TAE+IL-12), Th17 conditions (TAE+IL-1/IL-6/IL-21/IL-23/TGF-β), or Th2 conditions (TAE+IL-4). The production of IFN-γ, IL-17F and IL-10 was measured with cytometric bead arrays, in cell culture supernatants, after 5 days. **C)** Naïve and memory CD4^{+} T cells from healthy controls, two IL-12Rβ2-Q138X (P1 and P2), one IL-23R-C115Y (P4) and four IL-12Rβ1-deficient patients were stimulated with TAE beads, and cytokine production was measured 5 days later. Data for the production of IFN-γ, TNF and IL-2 are shown in the upper panels and for IL-17A, IL-17F and IL-10 in the lower panels.

Figure 4: Specific defects in the IL-12- and IL-23-dependent generation of an IFN-γ immune response in patients with novel homozygous mutations of *IL12RB2* or *IL23R*.

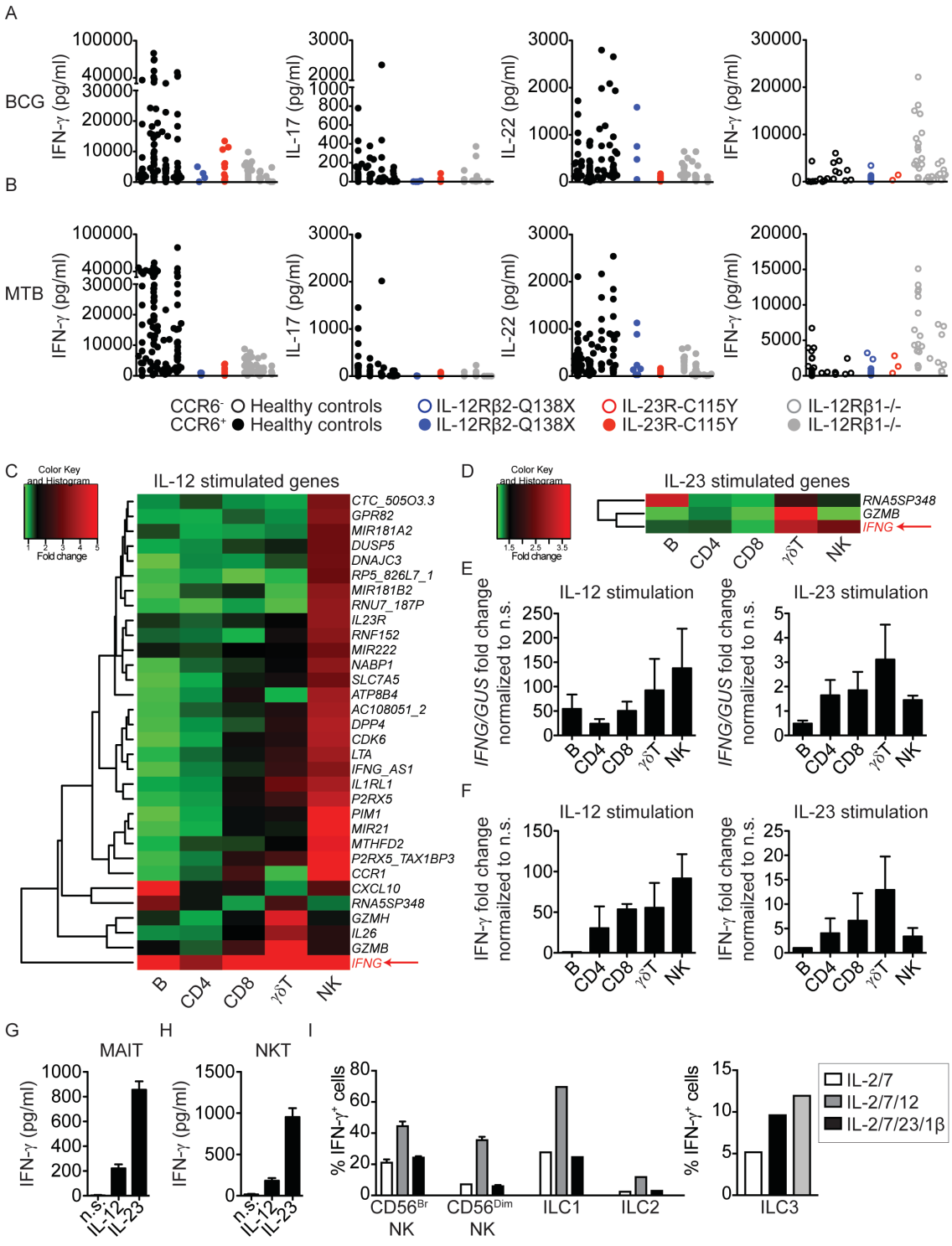

A, B) Multiple $CCR6^+$ or $CCR6^-$ memory $CD4^+$ T-cell lines were generated by the polyclonal stimulation of sorted peripheral blood subsets from healthy controls (*n*=4), one IL-12Rβ2-Q138X patient, one IL-23R-C115Y patient, and three IL-12Rβ1-deficient patients. Lines were screened for reactivity with peptide pools covering antigens from BCG (upper panel) and MTB (lower panel). BCG- and MTB-reactive $CD4^+CCR6^+$ T-cell lines from each individual were selected and the cytokines accumulating in the culture supernatant were determined with a Luminex machine. Each dot on the graph corresponds to a value for a single antigen-reactive T-cell line. $CCR6^+$ T-cell lines are shown as closed circles, and $CCR6^-$ cell lines are shown as open circles. **C, D)** Microarray heat map of isolated B, $CD4^+$ T, $CD8^+$ T, $\gamma\delta^+$ T and NK cells stimulated with IL-12 (C) or IL-23 (D) for 6 h. The data shown are the fold-induction relative to non-stimulated (n.s.) cells. The most commonly upregulated gene, *IFNG*, is highlighted in the lower right corner of each heat map. **E)** *IFNG* induction by isolated B, $CD4^+$ T, $CD8^+$ T, γδT, and NK cells from 5 healthy controls, upon stimulation with IL-12 or IL-23 for 6 h, was assessed by qPCR, and the data were normalized relative to n.s. cells. **F)** IFN-γ levels in the supernatants from the cells used in (E) were analyzed by ELISA and represented as a fold-change, relative to n.s. cells. **G, H)** Sorted MAIT cells (G) or NKT cells (H) (>95% pure) were left unstimulated, or stimulated with rhIL-12 (20 ng/mL) or rhIL-23 (100 ng/mL) for 6 h. Cell culture supernatants were harvested and used for IFN-γ determination in a multiplex cytokine assay. **I)** NK cells, ILC1, or ILC2 were sorted, by FACS, from blood samples from healthy donors and cultured in the presence of the indicated cytokines for 24 h. Total ILCs were gated on viable $CD45^+Lin^-$ ($CD3^-CD4^-CD5^-TCR\alpha\beta^-TCR\gamma\delta^-CD14^-CD19^-$) $CD7^+$ cells. NK cells were identified as $CD56^{bright}$ and $CD56^{dim}$, ILC2 as $CD56^-CD127^+CRTh2^+$ and

ILC1 as $CD56^{-}CD127^{+}CD117^{-}CRTh2^{-}$. IFN-γ levels were determined by intracellular staining. ILC3 were sorted by FACS from the tonsillar tissues of healthy donors, by gating on viable $CD45^{+}$ $Lin^{-}CD7^{+}CD117^{+}NKp44^{+}$ cells. ILC3 were cultured for 4 days in the presence of the indicated cytokines, and IFN-γ was then determined by intracellular staining.

Supplementary Online Materials

Ethics statement

This study was conducted in accordance with the Helsinki Declaration, with written informed consent obtained from the patients' families. Approval for this study was obtained from the French Ethics Committee "Comité de Protection des Personnes" (CPP), The French National Agency for Medicine and Health Product Safety (ANSM) and the *Institut National de la Santé et de la Recherche Médicale* (INSERM) in France, and the Rockefeller University Institutional Review Board (IRB), New York, USA.

Case Reports

Kindred A: P1 was born in 2008 to first-cousin consanguineous parents from Turkey (Fig. 1A, III.2). She was vaccinated with BCG at the age of three months and presented left axillary lymphadenitis (5 cm x 5 cm) at 17 months of age. A tuberculin skin test was strongly positive (PPD = 20x20 mm). Initial hemoglobin concentration was 11.8 g/dl, WBC was 13,000/mm^3, absolute neutrophil count was 7,000/mm^3, and absolute lymphocyte count was 4,700/mm^3. Tests for HIV antibody were negative. Serum immunoglobulin levels were normal. Peripheral blood lymphocyte subsets and *in vitro* T-

cell functions were normal. Neutrophil function was normal in terms of respiratory burst, tested in the DHR assay (upon PMA activation). CD212 (IL-12Rβ1) expression was normal (CD212: 93% of leukocytes). Chest X-ray findings were normal. Pathology examinations of the lymph node capsule biopsy specimen revealed caseating granulomatous inflammation. Ziehl-Neelsen staining for acid-fast bacilli (AFB) detected such bacilli within histiocytes. *M. tuberculosis* infection could not be confirmed by diagnostic PCR and the *Mycobacterium bovis*-BCG vaccine was suspected. Ziehl-Neelsen staining for AFB was negative for a gastric aspirate sample. The patient was diagnosed with BCG-osis and treated with isoniazid, rifampin, ethambutol and clarithromycin. After two months, ethambutol and clarithromycin treatments were stopped, and isoniazid and rifampin were continued for six months. The patient made a full recovery and has never had *Salmonella* or *Candida* infections.

P2 was born, in 1989, to first-cousin consanguineous parents (Fig. 1A, II.3). P2 had pulmonary tuberculosis at the age of five years, for which he received anti-TB treatment (details not available) and recovered. He has never had *Salmonella* or fungal infections. His family history contains no other remarkable elements and P2 is healthy without treatment.

P3 was born in 1979 and is asymptomatic. P2 and P3 are the uncles of P1.

Kindred B: P4 was born in 1994, to consanguineous parents from Iran (Fig. 1B, II.1). P4 was vaccinated with BCG in early infancy and developed BCG-adenitis with pus discharge, which persisted for one year and then spontaneously resolved. She is now well, with no treatment. Her younger brother, P5, was born in 2006 (Fig. 1B, II.5). He was also vaccinated with BCG in early infancy, after which he developed axillary lymphadenopathy

that did not resolve. At the age of five years, he was admitted to hospital for hepatosplenomegaly and mediastinal lymphadenopathy. He was treated with an antimycobacterial drug regimen, including isoniazid, rifampicin, ethambutol, ofloxacillin, clarythromysin, cycloserine, and dapsone, for 1.5 years. He was also treated with exogenous IFN-γ therapy. PPD testing at the age of seven years was negative. From the age of seven years, P5's infection progressed despite treatment, and he died of disseminated BCG disease at the age of eight years.

Materials and Methods

Genome-wide linkage (GWL) analysis: GWL analysis was performed as previously described (*53*), with minor modifications. For Kindred A, P1 was genotyped with the Affymetrix Genome-Wide Human SNP array 6.0, and six other individuals (P2, P3, II.5, II.6, III.1, III.3) were genotyped with the Affymetrix Genome-Wide Human SNP array 250K. For Kindred B, all seven individuals shown in the pedigree (Fig. 1B) were genotyped with the Affymetrix Genome-Wide Human SNP array 250K. Genotype was called with the Affymetrix Power Tools software package (http://www.affymetrix.com/estore/partners_programs/programs/developer/tools/powertools.affx). SNPs presenting more than one Mendelian inconsistency were discarded and the remaining SNPs were filtered with population-based filters (*54*). For Kindred A, we used 164,052 SNP markers for linkage analysis, assuming AR inheritance with 75% penetrance, and a deleterious allele frequency of 10^{-4}. For Kindred B, we used 162,563 SNP markers for linkage analysis, assuming AR inheritance with 75% penetrance, and a deleterious allele frequency of 10^{-4}. The penetrance estimate was based on the known clinical

penetrance of IL-12Rβ1 deficiency (*6*, *7*). Parametric multipoint linkage analysis was carried out independently for each kindred with the Merlin program (*55*), considering the founders to be second-degree relatives. The family founders and HapMap CEU trios were used to estimate allele frequencies and to define linkage clusters, with an r^2 threshold of 0.4.

Principal component analysis (PCA): PCA was conducted using whole exome sequencing (WES) data of 3752 individuals of diverse ethnic origins from our in-house exome database and 2504 unaffected individuals of the 1000 Genomes Project as reference individuals, as described (*24*). The analysis was restricted to variants covered by the exome capture Agilent's SureSelect V1 with a MAF greater than 5%. The principal components were obtained using the software PLINK (*54*).

Whole-exome sequencing (WES): Genomic DNA was prepared from blood samples from P1, P2, P3, P4 and P5. The DNA was sheared with a Covaris S2 Ultrasonicator (Covaris), and an adapter-ligated library was prepared with the Paired-End Sample Prep kit V1 (Illumina). Exome capture was performed with the Aligent SureSelect Human Exome kit (71 Mb version), according to the manufacturer's instructions. Exome sequencing was performed by the New York Genome Center, on an Illumina HiSeq 2500 machine. The reads were aligned to the human reference genome with BWA (*56*), then recalibrated and annotated with GATK (*57*), PICARD (http://picard.sourceforge.net/) and ANNOVAR (*58*). Substitution calls were made with GATK UnifiedGenotyper, whereas indel calls were made with SomaticIndelDetectorV2. All calls with a read coverage <2x and a Phred-scaled

SNP quality of <20 were filtered out. The variants were further filtered and investigated with our in-house online server (*59*). All *IL12RB2* and *IL23R* mutations identified by WES were confirmed by Sanger sequencing. Familial segregation analysis was performed in both families, when the necessary material was available.

Population genetic analyses: We estimated the strength of the purifying selection acting on *IL12RB1*, *IL12RB2* and *IL23R* in humans, using an approach based on polymorphism and divergence data from synonymous and nonsynonymous sites within genes (*i.e.*, the McDonald-Kreitman table). This method, known as SnIPRE (*29*), uses a generalized linear mixed model to model genome-wide variability for categories of mutations and estimates two key population genetic parameters for each gene: γ, the population selection coefficient, and *f*, the proportion of nonsynonymous mutations that are non-lethal. We focused our investigation on the *f* parameter, which quantifies the strength of purifying selection acting on human genes (*i.e.*, the removal of deleterious alleles from the general population). The *f* parameter thus varies from 0 (all nonsynonymous mutations in the gene are lethal) to 1 (all nonsynonymous mutations in the gene are non-lethal). We first retrieved the alignment of the hg19 human genome and the PanTro3 chimp genome from UCSC Genome Browser. All differences between the two species were annotated functionally by snpEff (*60*), using the GRCh37.65 build. We retrieved all human CDS >20 bp long and considered, for each gene, the longest transcript available. We deduced the proportion of synonymous and non-synonymous sites in the 22,616 coding DNA sequences (CDS) obtained, accounting for gaps in human-chimp alignments. We then retrieved all polymorphisms identified in the WES data of phase 1 of the 1,000 Genomes Project (*30*).

We analyzed SNPs that were annotated as non-synonymous or synonymous, outside of gaps in the human-chimp alignment and polymorphic in at least one human population. We also removed from positions divergent between humans and chimps those that were actually polymorphic in humans or chimps, using the dbSNP136 chimp database. We finally obtained the number of divergent and polymorphic synonymous and nonsynonymous mutations, and the proportion of synonymous and nonsynonymous sites, in a total of 18,969 genes. SnIPRE was then used to estimate the *f* parameter, and genes of interest were ranked on the basis of *f* estimations.

Cell culture: The B-lymphoblastoid cell line (LCL-B) endogenously negative for IL-12Rβ2 and IL-23R expression, positive for IL-12Rβ1, STAT3, and engineered to express STAT4-iresGFP in a stable manner used, referred to hereafter as LCL-B^{STAT4}, has been described elsewhere (*27*). T-cell lines were generated by infecting peripheral blood mononuclear cells (PBMCs) from healthy controls or patients with *Herpesvirus saimiri*, as previously described (*61*). *Herpesvirus saimiri*-immortalized T (HSV-T) cells were cultured with a 1:1 mixture (by volume) of RPMI and Panserin 401 (Panbiotech), supplemented with 10% fetal bovine serum (FBS), 350 µg/ml glutamine, 100 c/ml gentamycin, and 10 U/ml hIL-2 (Roche). Phoenix-A packaging cells (ATCC) were cultured in IMDM medium (Gibco) supplemented with 10% FCS. B-LCL^{STAT4}, Epstein-Barr virus-transformed B cells (EBV-B cells), and PBMCs were cultured in RPMI supplemented with 10% FCS. In other experiments, 300,000 HEK293T cells/well were seeded in 6-well plates. The next day, 5 µg of pcDNA3.1-empty vector or pcDNA3.1 containing a C-terminally V5-tagged WT or Q138X *IL12RB2* were transfected in the presence of Lipofectamine reagent (Invitrogen),

per manufacturer's instructions. After 48 h, whole cell lysates (100 μg protein per lane) were subjected to SDS-PAGE electrophoresis in a 10% acrylamide/bisacrylamide gel, and the resulting bands were transferred to a PVDF membrane (Immobilon-P, Millipore). The membrane was then probed with antibodies directed against V5 (460708: Invitrogen), and GAPDH (G-9: Santa Cruz).

Production of retroviral particles: Plasmids containing the WT human *IL12RB2* (Origene #SC119132) or *IL23R* (Origene #RG211477) ORFs were obtained, and different alleles were generated by site-directed mutagenesis, with specific primers and the PFU II Hotstart PCR Master Mix (Agilent Technologies), according to the manufacturer's instructions. These ORFs were introduced into the pLZRS-IRES-ΔNGFR vector and used to generate retroviral particles, as previously described (*62*). Briefly, 10 μg of the retroviral vector pLZRS-IRES-ΔNGFR (empty vector), or the same vector backbone containing one of the insert sequences WT *IL12RB2*-V5, WT *IL23R*-V5, or one of the variants functionally characterized in this report, was used to transfect Phoenix-A packaging cells (ATCC) in the presence of the X-treme Gene 9 transfection reagent (Roche), according to the manufacturer's protocol. The ΔNGFR ORF encodes a truncated nerve growth factor receptor (NGFR, also known as CD271) protein that cannot transduce signal, which serves as a cell surface tag in this system. Transfected Phoenix-A cells were cultured with 2 μg/ml puromycin (Gibco) until all cells expressed ΔNGFR on their surface, as shown by flow cytometry with a PE-conjugated mouse anti-human NGFR antibody (BD Pharmingen). Phoenix-A packaging cells were cultured for another 24 h in the presence 2 μg/ml puromycin. The medium was then changed and the puromycin was removed. The virus-

containing culture supernatant was collected 24 h later. Retroviruses were concentrated from the culture supernatant with Retro-X Concentrator (Clontech), according to the manufacturer's protocol, and stored at -80°C until use.

Retroviral transduction: HVS-T cells, EBV-B cells, or LCL-B^{STAT} cells were transduced with retroviral particles by spinoculation (*62*). Briefly, six-well non-tissue culture treated plates were coated by incubation for 24 h with 100 ng/ml of RetroNectin (Takara) diluted in PBS. The next day, the wells were washed with PBS and the viral supernatants were thawed and added to the empty wells, and the volume in each well was made up to 2 ml with medium. Plates were centrifuged at 800 x *g* for 30 min and 10^6 cells were added to each well. The plates were centrifuged for 5 min at 300 x *g* and incubated at 37ºC for 5 days before the assessment of transduction efficiency. Transduced cells were purified by MACS, using magnetic bead-conjugated anti-NGFR antibody (Miltenyi Biotec), according to the manufacturer's protocol, and purity was confirmed, by flow cytometry, to be >95%.

Western blotting to assess the activation of STAT3 and STAT4: LCL-B^{STAT4} cells that were non-transduced, or retrovirally transduced and stably expressing the desired IL-12Rβ2 or IL-23R proteins, were left unstimulated, or were stimulated with rhIL-12 (20 ng/ml; R&D Systems), rhIL-23 (100 ng/ml; R&D Systems) or rhIFN-α2b (10^5 units/mL, Intron-A®, Schering) for 30 min. The culture medium was removed, and the cells were washed with ice-cold PBS, and lysed in RIPA buffer (50 mM TRIS pH8, 1 mM EDTA, 150 mM NaCl, 0.5% sodium deoxycholate, 1% NP40, 0.1% SDS) supplemented with 100 mM sodium orthovanadate and Complete Mini protease inhibitor cocktail (Roche). Whole lysates (100

μg protein per lane) were subjected to SDS-PAGE electrophoresis in a 10% acrylamide/bisacrylamide gel, and the resulting bands were transferred to a PVDF membrane (Immobilon-P, Millipore). The membrane was then probed with antibodies directed against V5 (460708: Invitrogen), phospho-STAT3 Tyr705 (9145S: Cell Signaling), STAT3 (9139S: Cell Signaling), phospho-STAT4 Tyr693 (AF4319: R&D systems), STAT4 (C46B10: Cell Signaling), phospho-TYK2 Tyr1054/1055 (9321S: Cell Signaling), TYK2 (14193S: Cell Signaling), phospho-JAK2 Tyr1007/1008 (C80C3: Cell Signaling), JAK2 (D2E12 XP: Cell Signaling) and GAPDH (G-9: Santa Cruz).

Western blotting to assess IL-23R *N*-glycosylation: Protein lysates were prepared as described above, from LCL-B^{STAT4} cells that were non-transduced, or retrovirally transduced to express the WT or C115Y IL-23R V5-tagged proteins. Chemical inhibitors of *N*-glycosylation were used, as previously described (*28*, *63*). Briefly, cells were left untreated or were treated with 166 mM kifunensine (Toronto Research Chemicals). After 48 hours, cell lysates were prepared as described above. Protein samples were then left untreated or digested overnight at 37°C with endoglycosidase-H (EndoH; Biolabs) or peptide N-glycoside-F (PNGaseF; Biolabs) in the appropriate buffer. Immunoblotting was performed with antibodies directed against V5 (460708: Invitrogen), and GAPDH (G-9: Santa Cruz).

CXCL10 ELISA: LCL-B^{STAT4} cells that were non-transduced, or retrovirally transduced and stably expressing the desired IL-12Rβ2 or IL-23R proteins, were left unstimulated, or were stimulated with rhIL-12 (20 ng/ml; R&D Systems) or rhIL-23 (100 ng/ml; R&D

Systems) for 24 h. Cell-free supernatants were collected, and used for CXCL10 quantification by ELISA (Biolegend #439904), according to the manufacturer's protocol. Results are expressed as the fold-change difference between IL12- or IL-23-stimulated and non-stimulated cells, for each cell type.

Genetic rescue experiments: HVS-T cells were generated from the PBMCs of P1, and were left non-transduced, or transduced with retroviral particles produced with pLZRS-IRES-ΔNGFR (empty vector), or with a vector consisting of the same backbone plus WT *IL12RB2*-V5, as described above. EBV-B cells were generated from the PBMCs of P4, as described above. Cells were left non-transduced, were transduced with retroviral particles produced with pLZRS-IRES-ΔNGFR (empty vector), or with a vector containing the same backbone plus WT *IL23R*-V5, as described above.

IL12RB2 K649N mRNA splicing experiments: PBMCs were obtained from two healthy controls and a patient with a heterozygous *IL12RB2* mutation c.1947G>C, located in the first nucleotide of exon 15 and potentially causing both the K649N substitution and alternative splicing. Phytohemagglutinin (PHA)-blasts were generated by stimulating 2 x 10^6 PBMCs with 5 μg/ml PHA for 72 h. Total RNA was extracted from PHA-blasts or HVS-transformed T cells with TRIzol (Invitrogen), according to the manufacturer's protocol. We generated cDNA from 5 μg of total RNA, with the SuperScript First-Strand III Synthesis System for RT-PCR (Invitrogen). PCR was performed with primers binding between exons 12 and 15 of *IL12RB2* (5'-GCC CCG AGT GAC ATA TGT CA-3' and 5'-CTT TTT CCC TTT GTG GCC AG-3'). The PCR products were inserted into the pGEM-

T Easy vector (Promega, Madison, WI) and sequenced individually.

Ex vivo naïve and effector/memory $CD4^+$ T-cell stimulation: $CD4^+$ T cells were isolated as previously described (*64*). Briefly, cells were labeled with anti-CD4, anti-CD45RA, and anti-CCR7 antibodies, and naïve (defined as $CD45RA^+CCR7^+CD4^+$) or effector/memory (defined as $CD45RA^-CCR7^-CD4^+$) T cells were isolated (>98% purity) on a FACS Aria machine (BD Biosciences). Purified naïve or effector/memory $CD4^+$ cells were cultured with T-cell activation and expansion (TAE) beads (anti-CD2/CD3/CD28; Miltenyi Biotec) for 5 days, and culture supernatants were then used to assess the secretion of the cytokine indicated, by ELISA (IL-22) or in a cytometric bead array (all other cytokines).

In vitro differentiation of naïve $CD4^+$ T cells: Naïve $CD4^+$ T cells (defined as $CD45RA^+CCR7^+CD4^+$) were isolated (>98% purity) with a FACS Aria (BD Biosciences) machine from healthy controls or patients. They were then cultured under polarizing conditions, as previously described (*64*). Briefly, cells were cultured with TAE beads alone or under Th1 (IL-12 [20 ng/ml; R&D Systems]), Th2 (IL-4 [100 U/ml]; anti-IFN-γ [5 μg/ml; eBioscience]) was also included in some cultures) or Th17 (TGFβ, IL-1β [20 ng/ml; Peprotech], IL-6 [50 ng/ml; PeproTech], IL-21 [50 ng/ml; PeproTech], IL-23 [20 ng/ml; eBioscience], anti-IL-4 [5 μg/ml], and anti-IFN-γ [5 μg/ml; eBioscience]) polarizing conditions. After 5 days, culture supernatants were used to assess the secretion of the cytokines indicated, by ELISA (IL-22) or with cytometric bead arrays (all other cytokines).

T-cell libraries: Two subsets of $CD45RA^{-}CD25^{-}CD19^{-}CD8^{-}CD4^{+}$ memory T cells were sorted from total PBMC with a FACS Aria machine (BD Biosciences) on the basis of CCR6 expression. $CD45RA^{+}CCR7^{+}$ naïve cells were excluded. The $CCR6^{+}$ subset included Th1* and Th17 cells, whereas the $CCR6^{-}$ subset included Th1 and Th2 cells (*65*). The sorted memory $CCR6^{-}$ T cells were used to seed culture plates at a density of 600 cells/well, and $CCR6^{+}$ cells were used to seed plates at a density of 150-300 cells/well. The cells were cultured in RPMI 1640 medium supplemented with 2 mM glutamine, 1% (vol/vol) non-essential amino acids, 1% (vol/vol) sodium pyruvate, penicillin (50 U/ml), streptomycin (50 μg/ml) (all from Invitrogen) and 5% heat-inactivated human serum (Swiss Red Cross). All wells were polyclonally stimulated with 1 μg/ml PHA (Remel) in the presence of irradiated (45 Gy) allogeneic PBMCs as feeder cells (2.5×10^4 per well) and IL-2 (500 IU/ml), in a 96-well plate, and T-cell lines were expanded in the presence of IL-2, as previously described (*37*). After 13-16 days, a small volume of cells from three $CCR6^{-}$ or $CCR6^{+}$ lines from each patient were pooled and tested for their ability to produce IFN-γ, IL-17A, IL-22 or IL-4, by intracellular staining (ICS) after stimulation with PMA (200 nM) and ionomycin (1 μg/ml) (Sigma-Aldrich). The screening of the T cell lines was performed 18-22 days after initial stimulation, by culturing thoroughly washed T cells (2.5×10^5/well) with autologous irradiated B cells (2.5×10^4), with or without a three-hour pulse with different antigens, including the *M. tuberculosis* peptide pool (0.5 μg/ml/peptide, from A. Sette's laboratory, LJI, comprising 207 peptides), the BCG peptide pool (0.5 μg/ml/peptide, from A. Sette's laboratory, LJI, comprising 211 peptides), the respiratory syncytial virus (RSV) peptide pool (1 μg/ml/peptide, from A. Sette's laboratory, LJI, comprising 190 peptides), and influenza virus (Influvac vaccine).

Proliferation was assessed on day 4, after incubation for 16 h with 1 μCi/ml [^{3}H]-thymidine (GE Healthcare). Cytokine concentrations in the culture supernatants were determined after 48 h of stimulation, in Luminex multiplex cytokine assays (Thermo Fisher). Precursor frequencies were calculated from the number of negative wells, assuming a Poisson distribution, and are expressed per million cells (*66*).

Purification of the leukocyte population by magnetic-activated cell sorting (MACS): Age-matched healthy donor PBMCs were stained with microbead-conjugated antibodies directed against CD20, CD56, CD8 or CD4 (Miltenyi Biotec), according to the manufacturer's protocol, or biotin-conjugated anti-γδTCR (331206: Biolegend); they were then washed in PBS, then stained with anti-biotin microbeads (Miltenyi Biotec). Labeled cells were purified by passing the cell suspension through MS columns (Miltenyi Biotec) and retaining the eluate. The purity of each cell population was shown, by flow cytometry, to be ≥92%. Leukocytes were then stimulated with rhIL-12 (20 ng/ml; R&D Systems), rhIL-23 (100 ng/ml; R&D Systems), or PMA and ionomycin (20 μg/ml and 1 μM) for 6 h.

Leukocyte purification by FACS sorting: Healthy donor PBMCs were stained with Live/Dead fixable aqua (Invitrogen), anti-CD3 V450 (560365: BD Biosciences), anti-CD161 FITC (339923: Biolegend), anti-Vα24Jα PerCPeF710 (46-5806-42: eBiosciences) and anti-Vα7.2 APC (351724: Biolegend). MAIT cells were sorted on a FACS Aria II machine (BD Biosciences) with gating on $CD3^+CD161^+V\alpha7.2^+$ cells. NKT cells were sorted as $CD3^+V\alpha24J\alpha^+$ cells. Sorted MAIT or NKT cells (>95% purity) were then

stimulated with rhIL-12 (20 ng/ml; R&D Systems), rhIL-23 (100 ng/ml; R&D Systems), or PMA and ionomycin (20 μg/ml and 1 μM) for 6 h.

mRNA isolation, microarray, and quantitative RT-PCR: mRNA was prepared with the ZR RNA microprep kit (Zymo Research), according to the manufacturer's protocol. mRNA samples were used to prepare biotinylated ss-cDNA fragments with the GeneChip® Whole Transcript PLUS Reagent Kit (Affymetrix), which were then hybridized to a GeneChip® Human Transcriptome 2.0 array (Affymetrix), according to the manufacturers' instructions. Data were analyzed with Affymetrix® Expression Console™ and Transcription Analysis Console software. PBMCs from three other healthy age-matched donors were stimulated as described above, mRNA was isolated and reverse transcription-PCR was performed with oligo-dT primers, according to the manufacturer's protocol (Applied Biosystems, Foster City, CA). Quantitative real-time PCR (qPCR) was performed with Applied Biosystems Taqman assays and exon-spanning probes directed against *IFNG, IL12RB2, IL12RB1* and *IL23R*, with normalization against β-glucuronidase (*GUS*), glyceraldehyde 3-phosphate dehydrogenase (*GAPDH*), or 18S housekeeping genes.

Whole-blood activation experiments: Venous blood samples from healthy controls and from patients were collected into heparin-containing tubes and processed according a modified version of the procedure described by Feinberg et al. (*38*). Briefly, they were diluted 1:2 in RPMI1640 (GibcoBRL) supplemented with 100 U/ml penicillin and 100 μg/ml streptomycin (GibcoBRL). We dispensed 5 ml of diluted blood sample into each of 5 wells (1 ml/well) of a 48-well plate (Nunc). These samples were incubated for 48 h at

37°C, under an atmosphere containing 5% CO_2/95% air, and under three different sets of activation conditions: with medium alone, with live BCG (*M. bovis*-BCG, Pasteur substrain) at a MOI of 20 BCG bacteria/leukocyte, or with BCG plus recombinant (rh) IL-12 (20 ng/ml; R&D Systems). ELISA was performed on the collected supernatants, with the human IFN-γ ELISA Kit (Sanquin), according to the manufacturer's instructions.

PBMC activation experiments: PBMCs were isolated from buffy coats and used at a density of 10^6/ml in RPMI medium supplemented with 10% FBS. Cells were treated with rhIL-12 (20 ng/ml; R&D Systems), rhIL-23 (100 ng/ml; R&D Systems), or live BCG (*M. bovis* BCG, Pasteur substrain) at a MOI of 20 BCG cells/leukocyte, or PMA plus ionomycin (20 μg/ml and 1 μM) in for 48 h. All experiments were performed in triplicate wells. Cell culture supernatants were removed and used for multiplex cytokine detection with the V-PLEX Human Proinflammatory cytokine panel assay (Meso Scale Discovery).

Supplementary figure legends

Supplementary Figure 1: Clinical and genetic features of kindreds with autosomal recessive IL-12Rβ2 or IL-23R deficiency.

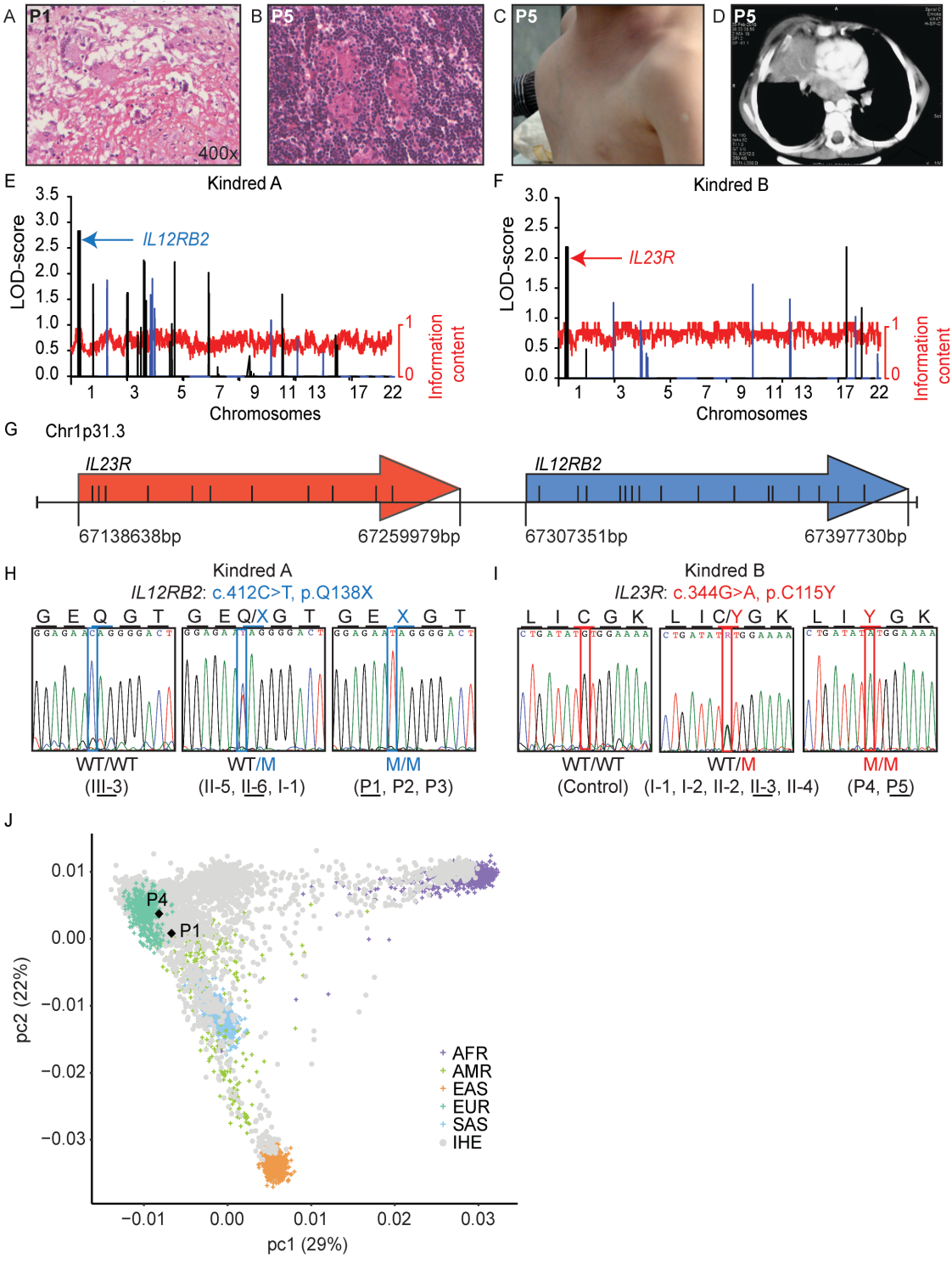

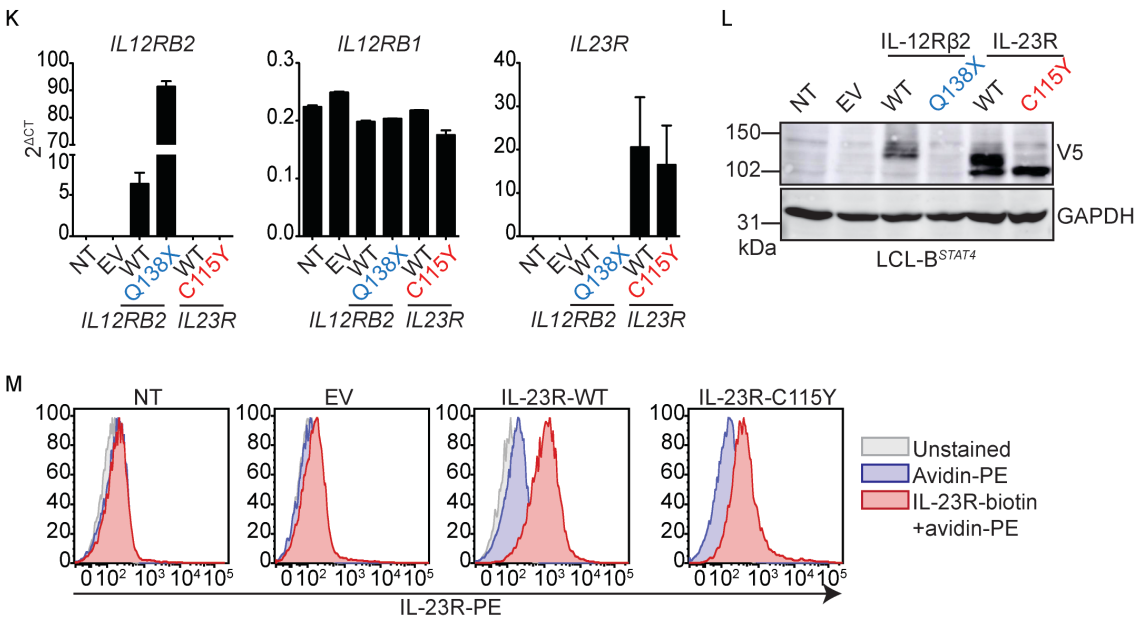

A) Histology of a lymph node biopsy specimen for P1 (IL-12Rβ2 Q138X) showing epithelioid and multinucleated giant cells at the periphery of a necrotic area. **B)** Histology of a lymph node biopsy specimen for P5 (IL-23R C115Y) showing follicular hyperplasia and the presence of small ill-defined macrophagic granulomas. **C)** Gross anatomical depiction of the chest mass resulting from *Mycobacterium bovis*-BCG infection in P5 at the age of four years. **D)** CT scan of the chest, cross-sectional view, showing a mediastinal mass, in P5 at the age of four years. **E, F)** Whole-genome linkage (WGL) analysis of kindred A (E) and kindred B (F). LOD scores are shown in black and blue for alternating chromosomes, and information content is shown with a red trace. Both *IL12RB2* and *IL23R* map to the linked region of chromosome 1 indicated with an arrow. **G)** Schematic representation of the region of chromosome 1 containing *IL12RB2* and *IL23R,* located head to tail. Each arrow represents a gene, *IL23R* in red and *IL12RB2* in blue. The direction of the arrow indicates the orientation of the gene on the chromosome. The locations of the first and last nucleotide of each gene are indicated underneath the diagram. The horizontal

line represents the corresponding part of chromosome 1 and the vertical lines within each arrow indicate exon positions. **H, I)** Representative electrophoretograms corresponding to a WT individual, a heterozygous carrier and a homozygous carrier of the *IL12RB2*-Q138X (H) and *IL23R*-C115Y (I) mutations. The electrophoretograms shown are from the underlined individuals in Fig 1A-B. **J)** Principal component analysis (PCA) was performed as explained in Materials and Methods using 2,504 individuals of the 1000 Genomes Project classified in 5 populations (African (AFR), American (AMR), East Asian (EAS), European (EUR), South Asian(SAS)), and 3752 individuals of diverse ethnic origin from our in-house exome database (IHE). The two affected index cases, P1 homozygous for *IL12RB2* Q138X, and P4 homozygous for *IL23R* C115Y are shown (black diamonds). The two patients are located within clusters of individuals of our in house database who share the same origin (Turkish, and Iranian, respectively). The proportions of the variance explained by principal components (PC)1 and PC2 are shown in parentheses. **K)** LCL-B^{STAT4} cells were either left non-transduced (NT) or were transduced with a retrovirus generated with an empty vector (EV) or with a vector containing the WT or mutant V5-tagged *IL12RB2* or *IL23R*. Levels of *IL12RB2*, *IL12RB1* and *IL23R* mRNA were determined by RT-qPCR. **L)** Western blot of lysates from the same cells as in (J) with antibodies against the V5-tag, and GAPDH as the loading control. **M)** LCL-B^{STAT4} cells either non-transduced (NT) or transduced with retroviruses generated with an empty vector (EV) or with vectors containing V5-tagged WT or C115Y mutant versions of *IL23R*. Cells were then left unstained (gray trace), or were stained with an avidin-PE antibody only (blue trace), or an IL-23R-biotin antibody, washed and stained with an avidin-PE anybody (red trace). PE fluorescence is shown on the *x*-axis.

Supplementary Figure 2: *IL12RB2* Q138X and *IL23R* C115Y mutations abolish the response of the encoded receptor to its cognate cytokine ligand.

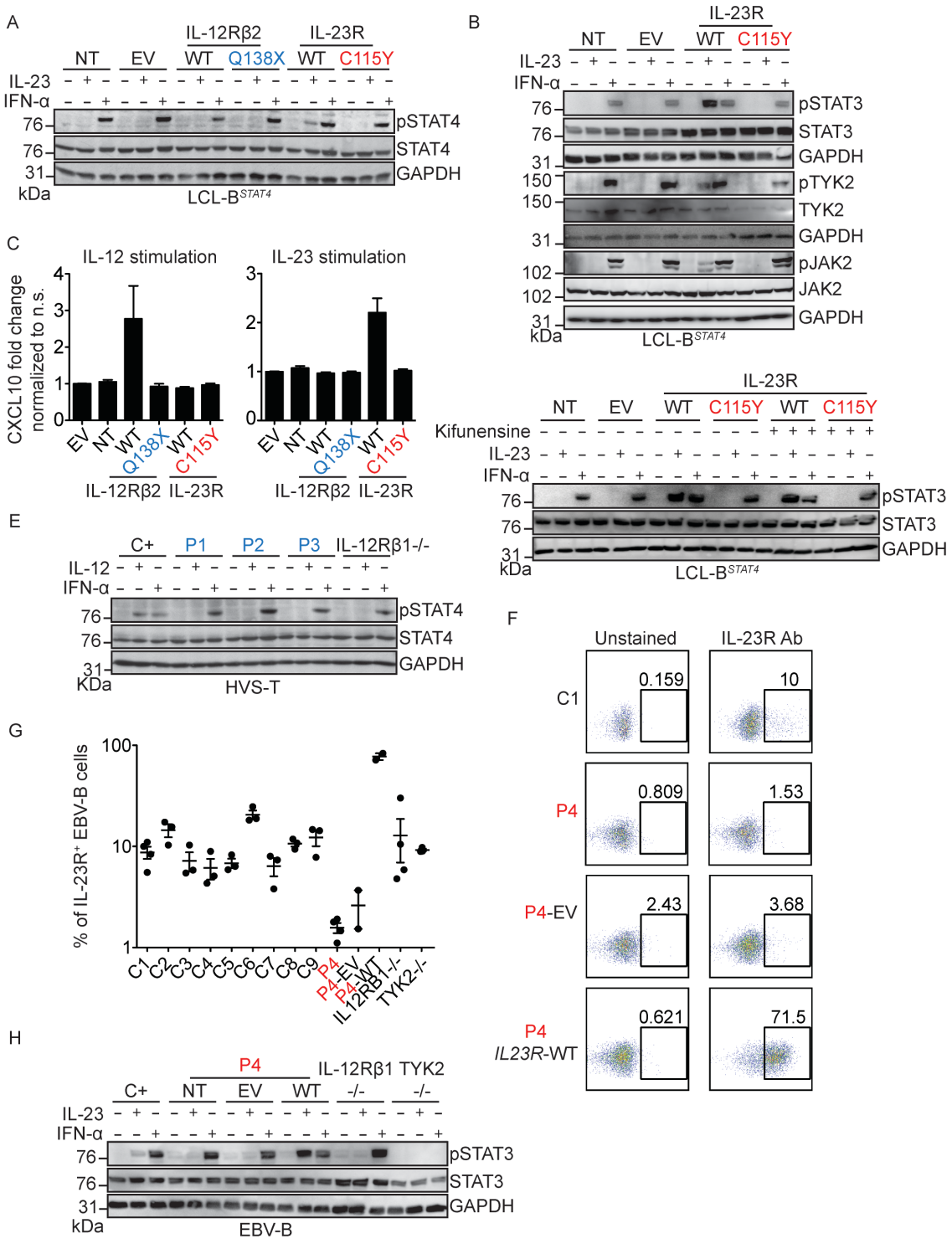

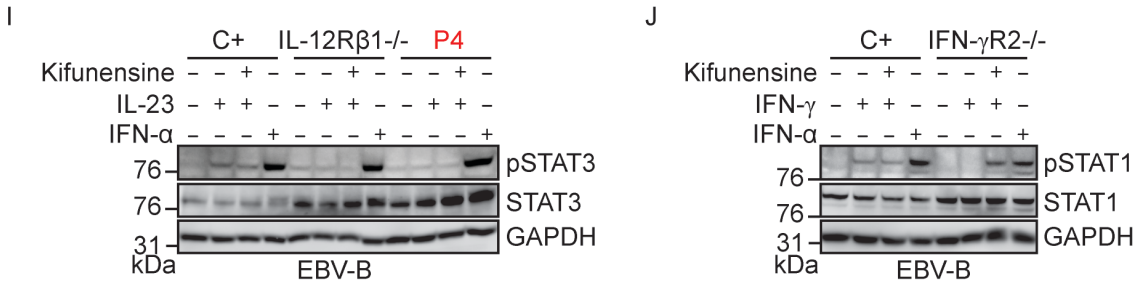

A) Western blot analysis of the same lysates as in Fig. 1I, with antibodies against phosphorylated STAT4, total STAT4 and GAPDH as a loading control. **B)** LCL-B^{STAT4} cells either non-transduced (NT) or transduced with retroviruses generated with an empty vector (EV) or vectors containing V5-tagged WT or C115Y mutant versions of *IL23R*, were either left unstimulated or were stimulated with IL-23 or IFN-α as a positive control. Lysates were analyzed by western blotting with antibodies against phosphorylated STAT3, total STAT3, phosphorylated TYK2, total TYK2, phosphorylated JAK2, total JAK2, and GAPDH as a loading control. **C)** LCL-B^{STAT4} cells were either left non-transduced (NT), or were transduced with retroviruses generated with an empty vector (EV) or vectors containing V5-tagged WT or Q138X mutant versions of *IL12RB2*, or WT or C115Y versions of *IL23R*. Cells were either left unstimulated, or stimulated with IL-12 or IL-23. After 24 h, the CXCL10 in the cell supernatant was determined by ELISA, and is expressed as a fold-change relative to unstimulated cells. **D)** The same cells as in (B) were either left unstimulated or were stimulated with IL-23 or IFN-α after 48 h of pretreatment with the glycosylation inhibitor kifunensine. Lysates were analyzed by western blotting with antibodies against pSTAT3, total STAT3 or GAPDH. **E)** HVS-T cells from a healthy control, the three IL-12Rβ2-deficient patients and an IL-12Rβ1-deficient patient were either left unstimulated or were stimulated with IL-12 or IFN-α as a positive control. They were then lysed and the lysates were subjected to western blotting with antibodies against

phosphorylated STAT4, total STAT4 and GAPDH as a loading control. **F)** FACS plots showing EBV-B cells from a representative healthy control, P4, P4 cells transduced with a retrovirus generated with an empty vector, or a vector containing WT *IL23R,* either unstained or stained for IL-23R. **G)** Percentage of EBV-B cells positive for IL-23R, for 9 healthy controls, P4, P4 cells transduced with a retrovirus generated with an empty vector (EV) or with a vector containing *IL23R-WT*, an IL-12Rβ- deficient patient and a TYK2-deficient patient. **H)** EBV-B cells from a healthy control (C+) P4, P4 cells transduced with a retrovirus containing *IL23R-WT*, an IL-12Rβ1-deficient patient and a TYK2-deficient patient were either left unstimulated or were stimulated with IL-23 or IFN-α as a positive control. The cells were lysed and the lysates were subjected to western blotting with antibodies against phosphorylated STAT3, STAT3 or GAPDH as a loading control. **I)** EBV-B cells from a healthy control, an IL-12Rβ1-deficient patient and P4 were either left unstimulated or were stimulated with IL-23 in the presence or absence of kifunensine. IFN-α stimulation was used as a positive control. Lysates were analyzed by western blotting with antibodies against phosphorylated STAT3, total STAT3 and GAPDH as a loading control. **J)** In parallel, as a control for kifunensine function, EBV-B cells from a healthy control and a patient carrying the loss-of-function *IFNGR2-382-387dup* mutation previously reported to be rescued by kifunensine treatment (*28*), were stimulated with IL-23 in the presence or absence of kifunensine, or with IFN-α as a positive control. The cells were lysed and the lysates were subjected to western blotting with antibodies against phosphorylated STAT1, total STAT1 and GAPDH as a loading control.

Supplementary Figure 3: Population genetics for *IL12RB1*, *IL12RB2* and *IL23R*.

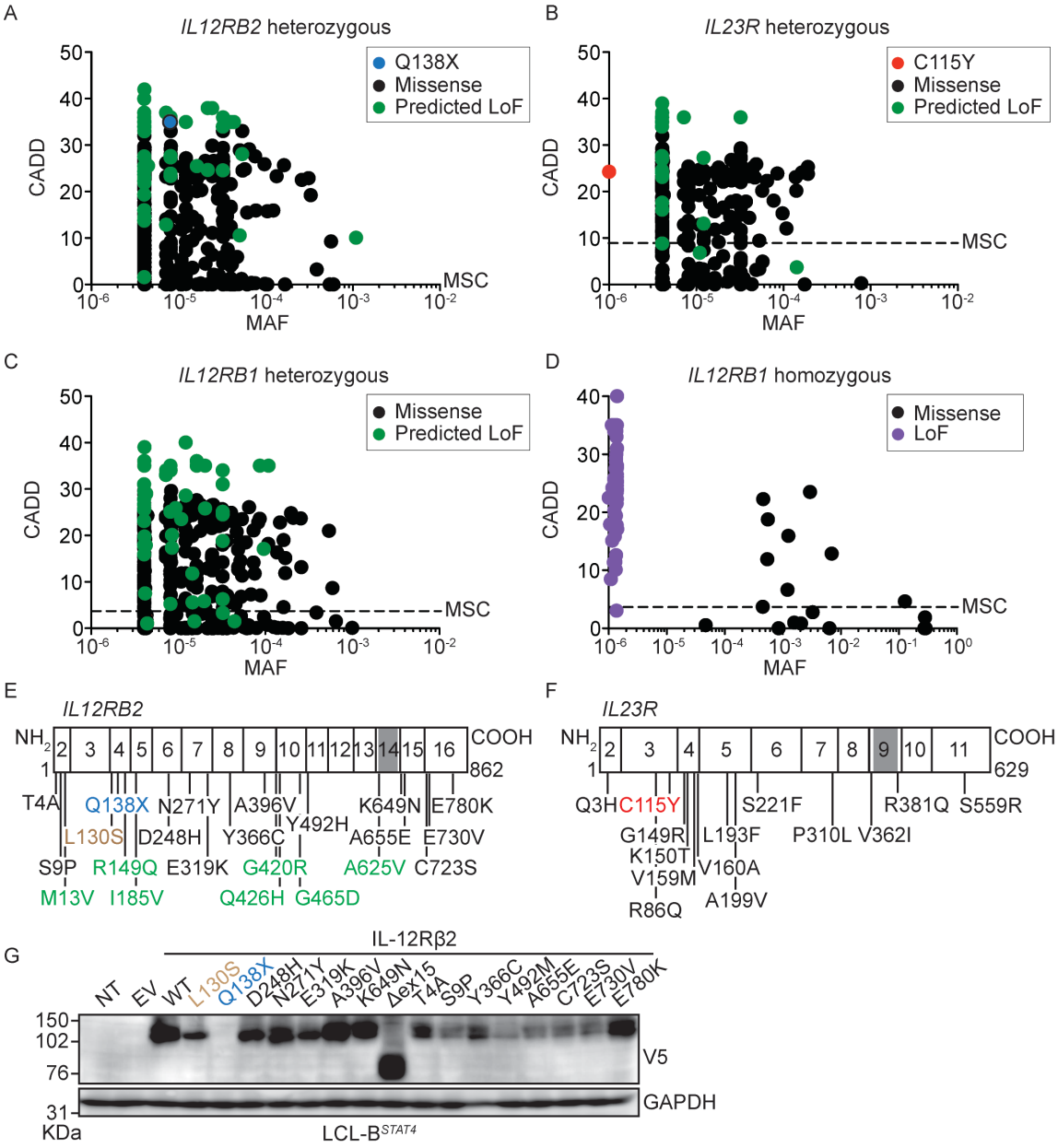

	PHA-blasts			HVS-T cells	
Allele	Control 1	Control 2	WT/K649N	Control 1	WT/K649N
WT	88%	90%	43.5%	87.5%	46.5%
Δex15	2.9%	8.6%	36.4%	11.5%	30.7%
K649N	0%	0%	12.9%	0%	13.9%
Others	9.1%	1.4%	7%	1%	8.9%
Colonies	34	70	85	96	101

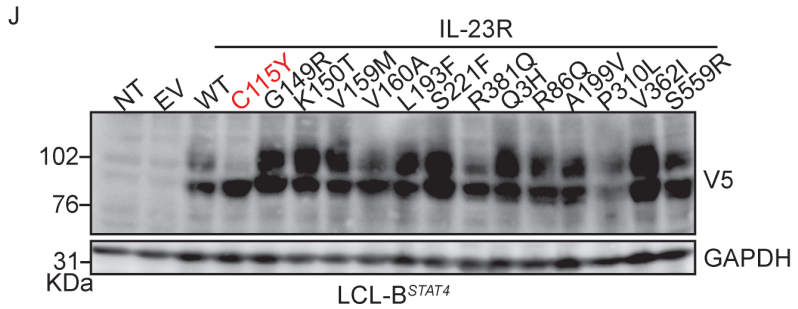

A) CADD score (*y*-axis) vs. minor allele frequency (MAF, *x*-axis) for all the heterozygous variants of *IL12RB2* found in gnomAD. The mutation studied here (Q138X) is shown in blue. Missense variants are shown in black and variants predicted to be loss-of-function (LOF; stop loss, start loss, nonsense, inframe indels, frameshift indels and essential splicing) are shown in green. **B)** CADD score (*y*-axis) vs. MAF (*x*-axis), for all the heterozygous variants of *IL23R* found in gnomAD. The mutation studied here (C115Y) is shown in red. Missense variants are shown in black and variants predicted to be LOF (stop loss, start loss, nonsense, inframe indels, frameshift indels and essential splicing) are shown in green. **C, D)** CADD score (*y*-axis) vs. MAF (*x*-axis) for all the heterozygous (C) and homozygous (D) variants of *IL12RB1* found in gnomAD. Missense variants are shown in black, and variants predicted to be LOF (stop loss, start loss, nonsense, inframe indels, frameshift indels and essential splicing) are shown in green. Variants previously demonstrated to impair or abolish IL-12Rβ1 function (LoF) are shown in purple. **E)** Schematic representation of IL-12Rβ2. Rectangles represent individual exons of the gene, with exon numbers indicated within the rectangles. The N-terminal portion of the protein is the extracellular domain, and gray shaded areas represent the transmembrane domain. The Q138X mutation identified in kindred A is shown in blue. *IL12RB2* variants tested by de Paus *et al.* and shown to be functional are shown in green (*27*). The L130S variant,

which is LOF (refer to Fig. 2E) is shown in orange and all the other variants present in the homozygous state in the gnomAD database are shown in black. **F)** Schematic representation of IL-23R. Rectangles represent individual exons of the gene with the exon numbers indicated within the rectangles. The N terminal portion of the protein is the extracellular domain, and gray shaded areas represent the transmembrane domain. The C115Y mutation identified in kindred B is shown in red. Variants present in the homozygous state in the gnomAD database are shown in black. **G)** LCL-B^{STAT4} cells were either left non-transduced (NT) or were transduced with a retrovirus generated with an empty vector (EV), a vector containing WT *IL12RB2,* or vectors containing all the homozygous *IL12RB2* variants reported in gnomAD and represented in Fig. 2C plus a plasmid containing the gene sequence but with the deletion of exon 15 described in (H, I). Lysates from these transduced cells were analyzed by western blotting with antibodies against the V5-tag and GAPDH as the loading control. **H)** cDNA was prepared from HVS-T cells from a WT donor, and from an individual heterozygous for the *IL12RB2* variant c.1947G>C. This variant may cause alternative splicing and the K649N substitution. The cDNA was amplified by PCR with primers specific to exons 14 and 16. The PCR product from HVS-T cells heterozygous for *IL12RB2* c.1947G>C gave an additional band of lower molecular weight than the WT individual, and this band corresponded to the skipping of exon 15 (Δex15). **I)** Using the same primers as in (H), RT-PCR was performed on PHA blasts from two WT and one heterozygous carrier of c.1947G>C, and HVS-T cells from a WT individual and a heterozygous carrier of c.1947G>C. PCR products were inserted into a pGEM-T easy vector that was then used to transform competent bacteria. Individual colonies were grown, and plasmid DNA was extracted and sequenced. This table shows

the observed *IL12RB2* genotypes corresponding to the PCR products obtained. **J)** LCL-B^{STAT4} cells were either left non-transduced (NT) or were transduced with a retrovirus generated with an empty vector, a vector containing WT *IL23R,* or vectors containing the homozygous *IL23R* variants reported in gnomAD and represented in Fig. 2D. Lysates from these transduced cells were analyzed by WB with antibodies against V5-tag, and GAPDH as a loading control.

Supplementary Figure 4: Immunophenotype of IL-12Rβ2-, IL-12Rβ1- and IL-23R-deficient patients.

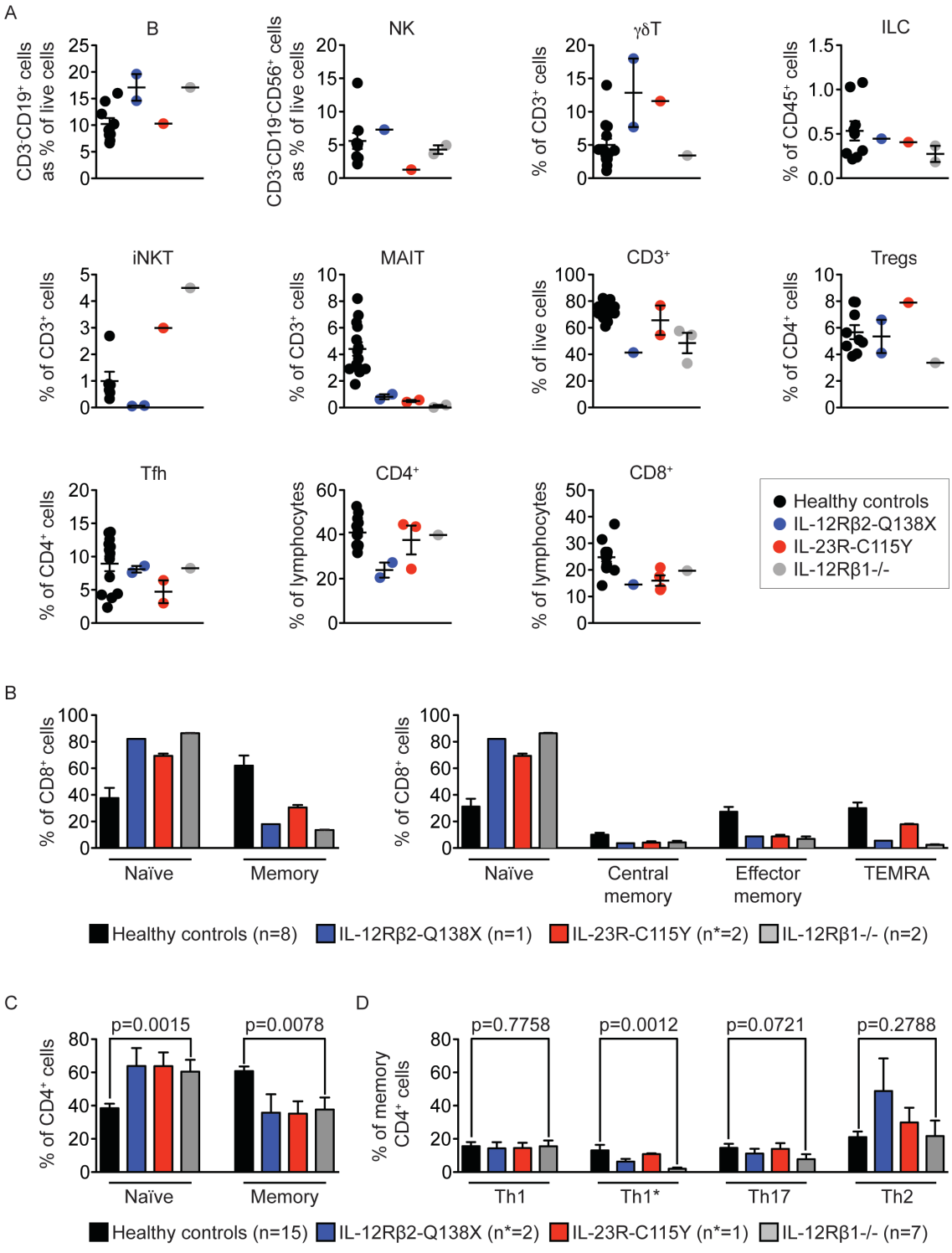

A) Frequencies of B, NK, γδT, ILC, NKT, MAIT, $CD3^+$, Tregs, Tfh, $CD4^+$ and $CD8^+$ cells for healthy controls (black), IL-12Rβ2-Q138X (blue), IL-23R-C115Y (red) and IL-12Rβ1-deficient patients (gray). **B)** On the left, frequencies of naïve and memory cells, as a percentage of total $CD8^+$ T cells. On the right, frequencies of naïve ($CCR7^+CD45RA^+$), central memory ($CCR7^+CD45RA^-$), effector memory ($CCR7^-CD45RA^-$) and T_{EMRA} ($CCR7^-CD45RA^+$) T cells as percentage of total $CD8^+$ T cells. Error bars indicate the SEM. **C)** Frequencies of naïve and memory cells, as a percentage of total $CD4^+$ T cells. **D)** Frequencies of four subsets of $CD4^+$ memory T cells ($CD3^+CD45RA^-$): Th1 ($CCR6^-CCR4^-CXCR3^+$), Th1* ($CCR6^+CCR4^-CXCR3^+$), Th17 ($CCR6^+CCR4^+CXCR3^-$) and Th2 ($CCR6^-CCR4^+CXCR3^-$) were measured and expressed as a percentage of total $CD4^+$ memory T cells ($CD3^+CD45RA^-$). Error bars indicate the SEM. P values for the comparison of healthy controls with *IL12RB1*$^{-/-}$ individuals in Mann-Whitney U-tests are shown.

Supplementary Figure 5: Non-antigen-specific cytokine production, and antigen-specific proliferation, precursor frequency, and cytokine production by $CD4^+$ memory T cells from healthy controls, IL-12Rβ2-, IL-23R- and IL-12Rβ1-deficient patients.

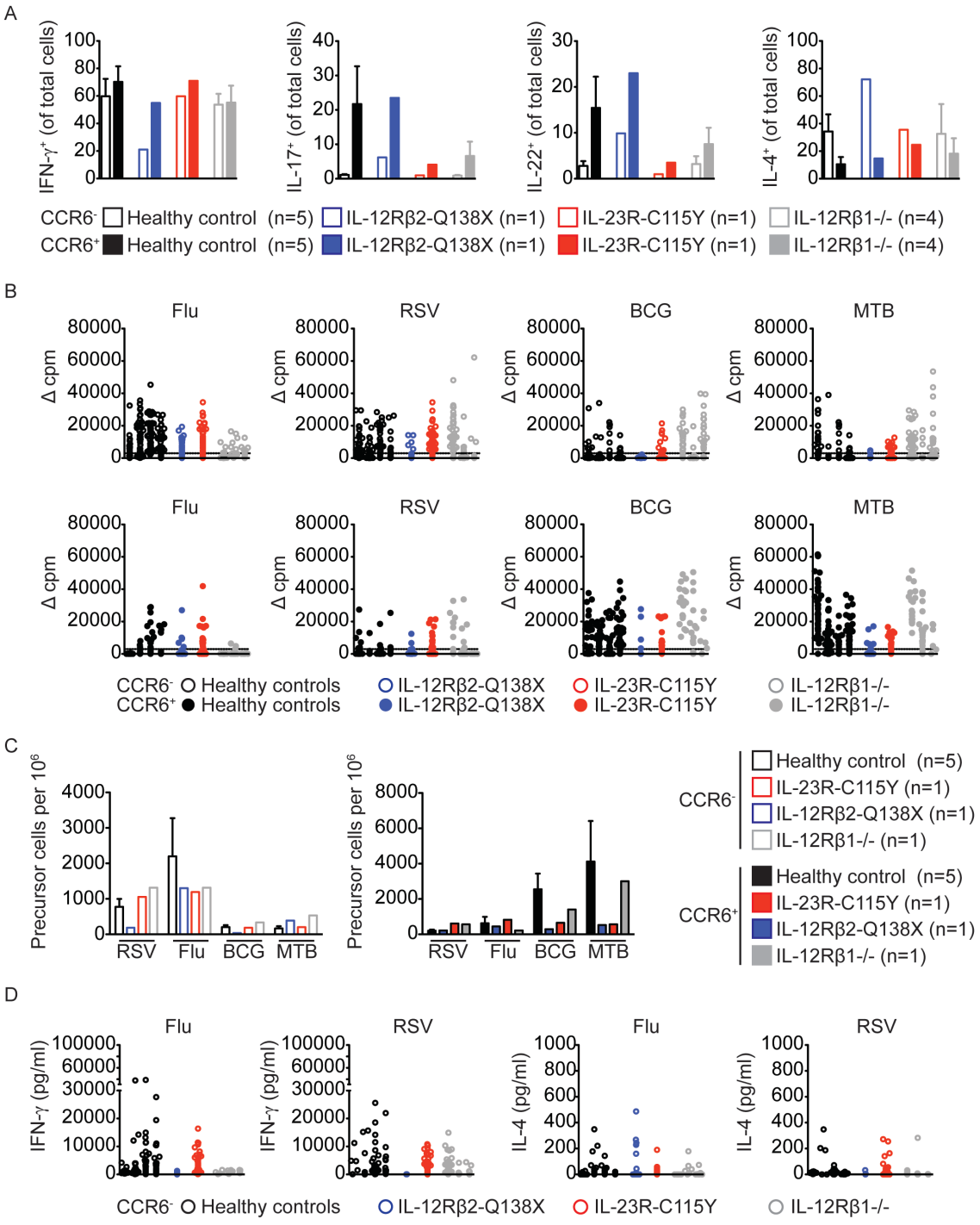

A) $CCR6^+$ or $CCR6^-$ memory $CD4^+$ T cell lines were generated from healthy controls (*n*=5), one IL-12Rβ2-Q138X patient, one IL-23R-C115Y patient, and four IL-12Rβ1-deficient patients. Stimulation with PMA + ionomycin was performed on pooled T-cell lines from each patient, and the frequency of cells positive for the indicated cytokines was assessed by intracellular flow cytometry. **B)** Proliferation, measured by 3H-thymidine incorporation, of $CD4^+CCR6^-$ (upper panels) and $CD4^+CCR6^+$ (lower panels) T-cell lines stimulated by autologous B cells pulsed with influenza virus, RSV, BCG or MTB peptide pools. Healthy controls are indicated in black, IL-12Rβ2-Q138X in blue, IL-23R-C115Y in red and IL-12Rβ1-deficient patients in gray. **C)** Frequency (mean number per million) of RSV-, influenza virus-, BCG- and MTB-specific memory T cells within the $CD4^+CCR6^-$ (left panel) and $CD4^+CCR6^+$ (right panel) subsets in healthy controls (black), IL-12Rβ2-Q138X (blue), IL-23R-C115Y (red) and IL-12Rβ1-deficient patients (gray), assuming a Poisson distribution. **D)** IL-4 and IFN-γ production by influenza virus- and RSV-specific $CD4^+CCR6^-$ memory T cells.

Supplementary Figure 6: Cytokine receptor expression and responses of MAIT and NKT cells to stimulation with IL-12 or IL-23.

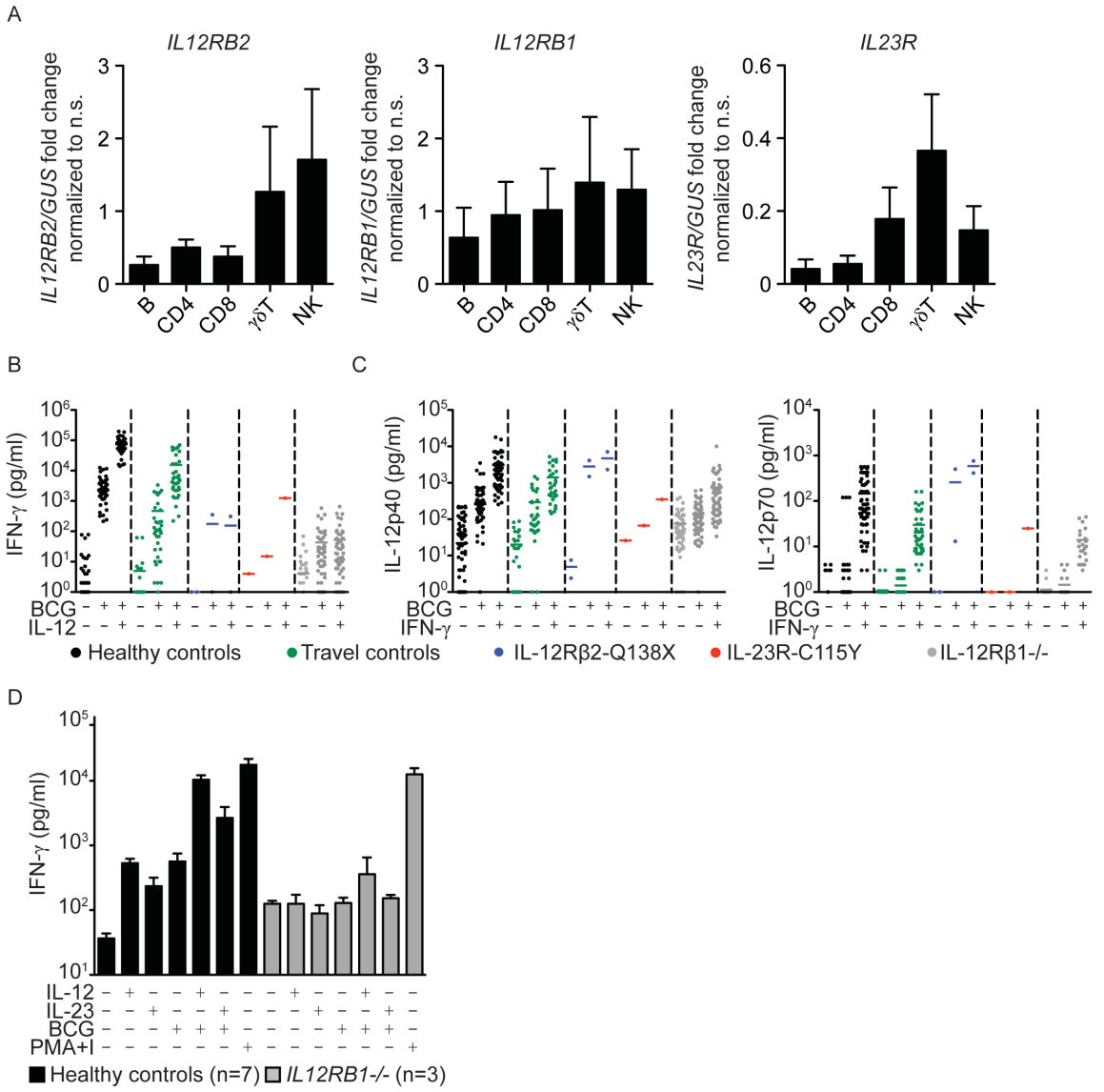

A) RT-qPCR for *IL12RB2*, *IL12RB1* and *IL23R* in B, CD4$^+$, CD8$^+$, γδT, NK, NKT and MAIT cells from Fig. 4E represented as relative expression, normalized against *GUS*. **B)** Whole blood was either left non-stimulated or was stimulated with IL-12, BCG or IL-12+BCG, and IFN-γ was determined 48 h after stimulation. **C)** Whole blood was either left non-stimulated or was stimulated with IFN-γ, BCG or IFN-γ +BCG, and IL-12p40 (left)

and IL-12p70 (right) were determined 48 h after stimulation. **D)** PBMCs from healthy controls and IL-12Rβ1-deficient patients were either left non-stimulated or were stimulated for 48 h with IL-12, IL-23, BCG, IL-12+BCG, IL-23+BCG or PMA+I, and IFN-γ was then determined.

References

1. J.-L. Casanova, Human genetic basis of interindividual variability in the course of infection. *Proc. Natl. Acad. Sci.* **112**, 201521644 (2015).
2. J.-L. Casanova, Severe infectious diseases of childhood as monogenic inborn errors of immunity. *Proc. Natl. Acad. Sci.* **1**, 201521651 (2015).
3. J.-L. Casanova, L. Abel, Genetic dissection of immunity to mycobacteria: The Human Model. *Annu. Rev. Immunol.* **20**, 581–620 (2002).
4. J. Bustamante, S. Boisson-Dupuis, L. Abel, J. L. Casanova, Mendelian susceptibility to mycobacterial disease: Genetic, immunological, and clinical features of inborn errors of IFN-γ immunity. *Semin. Immunol.* **26**, 454–470 (2014).
5. A. Y. Kreins *et al.*, Human TYK2 deficiency: Mycobacterial and viral infections without hyper-IgE syndrome. *J. Exp. Med.* **212**, 1641–1662 (2015).
6. L. de Beaucoudrey *et al.*, Revisiting Human IL-12Rβ1 Deficiency: a survey of 141 patients from 30 countries. *Medicine (Baltimore).* **89**, 381–402 (2011).
7. C. Fieschi *et al.*, Low Penetrance, Broad Resistance, and Favorable Outcome of Interleukin 12 Receptor β1 Deficiency. *J. Exp. Med.* **197**, 527–535 (2003).
8. S. Boisson-Dupuis *et al.*, Il-12rβ1 deficiency in two of fifty children with severe tuberculosis from IRN, MAR, and TUR. *PLoS One*. **6**, 1–7 (2011).
9. E. van de Vosse *et al.*, IL-12Rβ1 deficiency: Mutation update and description of the IL12RB1 variation database. *Hum. Mutat.* **34**, 1329–1339 (2013).
10. F. Altare *et al.*, Interleukin-12 receptor beta1 deficiency in a patient with abdominal tuberculosis. *J. Infect. Dis.* **184**, 231–236 (2001).
11. D. H. Presky *et al.*, A functional interleukin 12 receptor complex is composed of

two beta-type cytokine receptor subunits. *Proc. Natl. Acad. Sci. U. S. A.* **93**, 14002–7 (1996).

12. C. Parham *et al.*, A Receptor for the Heterodimeric Cytokine IL-23 Is Composed of IL-12R 1 and a Novel Cytokine Receptor Subunit, IL-23R. *J. Immunol.* **168**, 5699–5708 (2002).
13. M. W. L. Teng *et al.*, IL-12 and IL-23 cytokines: From discovery to targeted therapies for immune-mediated inflammatory diseases. *Nat. Med.* **21**, 719–729 (2015).
14. C. Prando *et al.*, Inherited IL-12p40 Deficiency. *Medicine (Baltimore)*. **92**, 109–122 (2013).
15. L. de Beaucoudrey *et al.*, Mutations in *STAT3* and *IL12RB1* impair the development of human IL-17–producing T cells. *J. Exp. Med.* **205**, 1543–1550 (2008).
16. A. Puel *et al.*, Chronic mucocutaneous candidiasis in humans with inborn errors of interleukin-17 immunity. *Science (80-.).* **332**, 65–68 (2011).
17. M. Ouederni *et al.*, Clinical features of candidiasis in patients with inherited interleukin 12 receptor β1 deficiency. *Clin. Infect. Dis.* **58**, 204–213 (2014).
18. V. Beziat *et al.*, A recessive form of hyper-IgE syndrome by disruption of ZNF341-dependent STAT3 transcription and activity. *Sci. Immunol.* **in press** (2018).
19. B. Boisson *et al.*, An ACT1 mutation selectively abolishes interleukin-17 responses in humans with chronic mucocutaneous candidiasis. *Immunity*. **39**, 676–686 (2013).

20. R. Lévy *et al.*, Genetic, immunological, and clinical features of patients with bacterial and fungal infections due to inherited IL-17RA deficiency. *Proc. Natl. Acad. Sci.* **113**, E8277–E8285 (2016).

21. J. Li, D. C. Vinh, J. L. Casanova, A. Puel, Inborn errors of immunity underlying fungal diseases in otherwise healthy individuals. *Curr. Opin. Microbiol.* **40**, 46–57 (2017).

22. Y. Ling *et al.*, Inherited IL-17RC deficiency in patients with chronic mucocutaneous candidiasis. *J. Exp. Med.* **212**, 619–631 (2015).

23. Y. Bloch *et al.*, Structural Activation of Pro-inflammatory Human Cytokine IL-23 by Cognate IL-23 Receptor Enables Recruitment of the Shares Receptor IL-12Rb1. **48**, 45–58.e6 (2018).

24. A. Belkadi *et al.*, Whole-exome sequencing to analyze population structure, parental inbreeding, and familial linkage. *Proc. Natl. Acad. Sci.* **113**, 6713–6718 (2016).

25. M. Kircher, A general framework for estimating the relative pathogenicity of human genetic variants. *Nat. Genet.* **46**, 310–315 (2014).

26. Y. Itan, L. Shang, B. Boisson, The mutation significance cutoff (MSC): gene-level thresholds for variant-level predictions Yuval. *Nat. Methods*. **13**, 109–110 (2016).

27. R. A. De Paus, M. A. Geilenkirchen, S. Van Riet, J. T. Van Dissel, E. Van De Vosse, Differential expression and function of human IL-12RB2 polymorphic variants. *Mol. Immunol.* **56**, 380–389 (2013).

28. G. Vogt *et al.*, Complementation of a pathogenic *IFNGR2* misfolding mutation with modifiers of N-glycosylation. *J. Exp. Med.* **205**, 1729–1737 (2008).

29. K. E. Eilertson, J. G. Booth, C. D. Bustamante, SnIPRE: Selection Inference Using a Poisson Random Effects Model. *PLoS Comput. Biol.* **8** (2012), doi:10.1371/journal.pcbi.1002806.

30. D. M. Altshuler *et al.*, An integrated map of genetic variation from 1,092 human genomes. *Nature*. **491**, 56–65 (2012).

31. Y. Itan *et al.*, The human gene damage index as a gene-level approach to prioritizing exome variants. *Proc. Natl. Acad. Sci.* **112**, 13615–13620 (2015).

32. S. Petrovski, Q. Wang, E. L. Heinzen, A. S. Allen, D. B. Goldstein, Genic Intolerance to Functional Variation and the Interpretation of Personal Genomes. *PLoS Genet.* **9** (2013), doi:10.1371/journal.pgen.1003709.

33. M. Deschamps *et al.*, Genomic Signatures of Selective Pressures and Introgression from Archaic Hominins at Human Innate Immunity Genes. *Am. J. Hum. Genet.* **98**, 5–21 (2016).

34. E. van de Vosse, R. A. de Paus, J. T. van Dissel, T. H. M. Ottenhoff, Molecular complementation of IL-12Rbeta1 deficiency reveals functional differences between IL-12Rbeta1 alleles including partial IL-12Rbeta1 deficiency. *Hum Mol Genet*. **14**, 3847–3855 (2005).

35. R. P. Wilson *et al.*, STAT3 is a critical cell-intrinsic regulator of human unconventional T cell numbers and function. *J. Exp. Med.* **212**, 855–864 (2015).

36. S. Okada, J. G. Markle, E. K. Deenick, F. Mele, Impairment of immunity to Candida and Mycobacterium in humans with bi-allelic RORC mutations. *Science (80-.).* **349**, 606–613 (2015).

37. R. Geiger, T. Duhen, A. Lanzavecchia, F. Sallusto, Human naive and memory

CD4+ T cell repertoires specific for naturally processed antigens analyzed using libraries of amplified T cells. *J. Exp. Med.* **206**, 1525–1534 (2009).

38. J. Feinberg *et al.*, Bacillus Calmette Guérin triggers the IL-12/IFN-γ axis by an IRAK-4- and NEMO-dependent, non-cognate interaction between monocytes, NK, and T lymphocytes. *Eur. J. Immunol.* **34**, 3276–3284 (2004).

39. C. Carpenter *et al.*, A side-by-side comparison of T cell reactivity to fifty-nine Mycobacterium tuberculosis antigens in diverse populations from five continents. *Tuberculosis*. **95**, 713–721 (2015).

40. F. Sallusto, Heterogeneity of Human CD4+ T Cells Against Microbes. *Annu. Rev. Immunol.* **34**, 317–334 (2016).

41. R. A. Kastelein, C. A. Hunter, D. J. Cua, Discovery and Biology of IL-23 and IL-27: Related but Functionally Distinct Regulators of Inflammation. *Annu. Rev. Immunol.* **25**, 221–242 (2007).

42. S. A. Khader *et al.*, IL-23 Is Required for Long-Term Control of *Mycobacterium tuberculosis* and B Cell Follicle Formation in the Infected Lung. *J. Immunol.* **187**, 5402–5407 (2011).

43. J. L. Flynn, An essential role for interferon gamma in resistance to Mycobacterium tuberculosis infection. *J. Exp. Med.* **178**, 2249–2254 (1993).

44. K. I. Happel *et al.*, Pulmonary interleukin-23 gene delivery increases local T-cell immunity and controls growth of Mycobacterium tuberculosis in the lungs. *Infect. Immun.* (2005), doi:10.1128/IAI.73.9.5782-5788.2005.

45. S. Hanna, A. Etzioni, MHC class I and II deficiencies. *J. Allergy Clin. Immunol.* **134**, 269–275 (2014).

46. J.-L. Casanova, E. Jouanguy, S. Lamhamedi, S. Blanche, A. Fischer, Immunological conditions of children with BCG disseminated infection. *Lancet*. **346**, 581 (1995).

47. L. Gineau *et al.*, Partial MCM4 deficiency in patients with growth retardation , adrenal insufficiency , and natural killer cell deficiency. *J Clin Invest*. **122**, 821–832 (2012).

48. J. Cottineau *et al.*, Inherited GINS1 deficiency underlies growth retardation along with neutropenia and NK cell deficiency. *J. Clin. Invest.* **127**, 1991–2006 (2017).

49. F. Vély *et al.*, Evidence of innate lymphoid cell redundancy in humans. *Nat. Immunol.* **17**, 1291–1299 (2016).

50. G. Chognard *et al.*, The dichotomous pattern of IL-12R and IL-23R expression elucidates the role of IL-12 and IL-23 in inflammation. *PLoS One*. **9** (2014), doi:10.1371/journal.pone.0089092.

51. D. I. Godfrey, A. P. Uldrich, J. Mccluskey, J. Rossjohn, D. B. Moody, The burgeoning family of unconventional T cells. *Nat. Immunol.* **16** (2015), doi:10.1038/ni.3298.1114.

52. C. S. N. Klose, D. Artis, Innate lymphoid cells as regulators of immunity, inflammation and tissue homeostasis. *Nat. Immunol.* **17**, 765–74 (2016).

53. A. V. Grant *et al.*, Accounting for genetic heterogeneity in homozygosity mapping: Application to mendelian susceptibility to mycobacterial disease. *J. Med. Genet.* **48**, 567–571 (2011).

54. S. Purcell *et al.*, PLINK: A Tool Set for Whole-Genome Association and Population-Based Linkage Analyses. *Am. J. Hum. Genet.* **81**, 559–575 (2007).

55. G. R. Abecasis, S. S. Cherny, W. O. Cookson, L. R. Cardon, Merlin — Rapid analysis of dense genetic maps using sparse gene flow trees. *Nat. Genet.* **30**, 97–101 (2002).

56. H. Li, R. Durbin, Fast and accurate long-read alignment with Burrows-Wheeler transform. *Bioinformatics*. **26**, 589–595 (2010).

57. A. Mckenna *et al.*, The Genome Analysis Toolkit : A MapReduce framework for analyzing next-generation DNA sequencing data The Genome Analysis Toolkit : A MapReduce framework for analyzing next-generation DNA sequencing data. *Genome Res.* **20**, 0–7 (2010).

58. K. Wang, M. Li, H. Hakonarson, ANNOVAR: Functional annotation of genetic variants from high-throughput sequencing data. *Nucleic Acids Res.* **38**, 1–7 (2010).

59. M. Byun *et al.*, Whole-exome sequencing-based discovery of STIM1 deficiency in a child with fatal classic Kaposi sarcoma. *J. Exp. Med.* **207**, 2307–2312 (2010).

60. P. Cingolani *et al.*, A program for annotating and predicting the effects of single nucleotide polymorphisms, SnpEff: SNPs in the genome of Drosophila melanogaster strain w1118; iso-2; iso-3. *Fly*. **6**, 80–92 (2012).

61. B. Biesinger *et al.*, Stable growth transformation of human T lymphocytes by Herpesvirus saimiri. *Proc. Natl. Acad. Sci.* **89**, 3116–3119 (1992).

62. R. Martínez-Barricarte *et al.*, *Curr. Protoc. Immunol.*, in press, doi:10.1002/cpim.15.

63. M. Moncada-Vélez *et al.*, Partial IFN-γR2 deficiency is due to protein misfolding and can be rescued by inhibitors of glycosylation. *Blood*. **122**, 2390–2401 (2013).

64. C. Ma *et al.*, Functional STAT3 deficiency compromises the generation of human

T follicular helper cells. *Blood*. **119**, 3997–4008 (2012).

65. E. V. Acosta-Rodriguez *et al.*, Surface phenotype and antigenic specificity of human interleukin 17-producing T helper memory cells. *Nat. Immunol.* **8**, 639–646 (2007).

66. I. Lefkovits, H. Waldmann, Limiting dilution analysis of cells of the immune system. **5**, 38–204 (1979).

Supplementary Table 1: Estimated proportions of deleterious and non-deleterious amino-acid variants in *IL12RB1*, *IL12RB2* and *IL23R*.

	IL12RB1	*IL12RB2*	*IL23R*
Fixed synonymous	9	11	7
Polymorphic synonymous	15	15	7
Fixed nonsynonymous	5	6	6
Polymorphic nonsynonymous	18	36	14
Synonymous sites	447.7	580	395.7
Nonsynonymous sites	1426.3	2009	1494.3
f estimate	46.7% [30.4% - 71.7%]	61.7% [42.1% - 90.3%]	49.0% [31.1% - 77.4%]
Genome-wide rank	50.0%	85.3%	57.0%
g estimate	-0.77 [-1.32 – -0.22]	-0.85 [-1.36 – -0.35]	-0.58 [-1.12 – -0.05]
Genome-wide rank	56.4%	47.9%	73.8%

Supplementary Table 2: Please refer to Auxiliary Supporting Materials and Other Supporting Files

Supplementary Table 3: Please refer to Auxiliary Supporting Materials and Other Supporting Files

Supplementary Table 4: Relative levels of IFN-γ production in response to IL-12 vs. IL-23 in different cell subsets.

Population	IL-12 (20 ng/ml)	IL-23 (100 ng/ml)
B	-	-
$CD4^+$ T	++	+
$CD8^+$ T	++	+
γδT	+++	++
NK	++++	+
MAIT	+	+++
NKT	+	+++
ILC1*	++	-
ILC2*	+	-
ILC3*	-	+

*Different stimulation conditions (as in Fig 4A)